공학박사 학위논문

Effect of Emitter Polarity on the Recombination Mechanism and Device Performance in Organic Light Emitting Diodes

유기발광다이오드에서 발광체의 극성이 재결합 기작과 소자 성능에 미치는 영향

2018년 2월

서울대학교 대학원

재료공학부

이 창 헌

Abstract

Effect of Emitter Polarity on the Recombination Mechanism and Device Performance in Organic Light Emitting Diodes

Chang-Heon Lee
Department of Material Science and Engineering
The Graduate School
Seoul National University

Recombination is a key process in organic optoelectronic devices. This phenomenon plays a central role in the formation of exciton in organic light emitting diodes (OLEDs), but it is a phenomenon to be minimized in the organic photovoltaics (OPVs) because it acts as the loss mechanism. There are two main recombination mechanisms considered in the organic semiconductors. One is bimolecular Langevin recombination that occurs between hole and electron and the other is trap assisted recombination that occurs between trapped charge and charge with opposite sign. The effect of each mechanism depends on the type of device, but understanding these phenomena is very important to enhance the performance of the devices. In dye-doped OLEDs that we studied, driving voltage and efficiency can be varied according to dominant recombination mechanism. Despite this importance, research on the factors that determine the recombination mechanism has not been done much. Effect of trap depth has been addressed so far, but it is reported that constructing Langevin dominant system with deep trap center of the emitter is possible. So a systematic study is needed on the factors that determine recombination phenomena.

Firstly, we studied virtual device which has features of exciplex forming co-host system (lower mobility in the emissive and barriers between emissive layer and adjacent layers.). We studied the effect of the interlayer barrier, the mobility of emissive layer and trap depth formed by the emitter on the recombination of OLEDs. With drift-diffusion modeling, we calculated charge density, recombination rate and portion of recombination in the device. As ϕ_{adj} increases, holes or electrons are accumulated at the interlayer surface. Also, decreasing μ_{EML} also result in charge accumulation at the emissive layer. Due to increased charge density in the devices, portion of Langevin recombination increased. However, ΔE_t is related to trapped hole density by affecting detrapping characteristics. This effect is saturated when ΔE_t is over 0.3 eV. Correspond this result to the exciplex system, we found that this system is a suitable platform to make Langevin dominant system.

Secondly, we report that the static dipole moment of the dopant is one of the most important factors influencing the recombination and emission mechanism in dye-doped OLEDs. Current-voltage and transient electroluminescence characteristics are mainly governed by the static dipole moment of the dyes in the emissive layer of OLEDs. Homoleptic Ir(III) dyes with large static dipole moment over 5 Debye induce trap-assisted-recombination dominated emission in OLEDs. However, heteroleptic Ir(III) dyes with small static dipole moment below 2 Debye lead to Langevin recombination dominated emission in OLEDs. Moreover, we considered the effect of dipole moment on trapping on the drift-diffusion model and this reveals that static dipole moment becomes a major factor determining the recombination mechanism in the dye-doped OLEDs when trap depth is higher than 0.25 eV where any de-trapping effect becomes negligible. This finding will be useful in various kinds of OLEDs including fluorescent or thermally assisted delayed fluorescent OLEDs where recombination sites play key roles.

Keywords: Recombination, drift-diffusion model, Langevin recombination, trap-assisted recombination, dipole moment of emitter
Student Number: 2013-30185

Contents

List of Tables

List of Figures

Chapter 1. Introduction

1.1 Organic Light Emitting Diodes

Organic light emitting diodes (OLEDs) have advantages for utilizing as displays and lightings such as the low cost of fabrication, lightweight, superior color quality and availability of flexible devices. Products including television and mobile display for the smartphone have already been released and many studies are still underway to develop new materials, improve their lifetime and efficiency.

An OLED is a planar device with a stacked structure, consisting of two electrodes including a transparent conducting electrode, charge injecting layers, charge transporting layers and an emissive layer. When the voltage is applied, the injected charge moves to the emissive layer through the injecting layer and the transporting layer, and recombination phenomenon occurs in the emissive layer which electrons and holes are combined, thereby emitting light through electroluminescence phenomenon. The external quantum efficiency (EQE) of OLEDs is express as in equation (1-1)[1], this means generated photons per injected electrons.

$$\eta_{EQE} = \eta_{\mathrm{int}} \times \eta_{out} = \gamma \times \eta_{S/T} \times q_{eff} \times \eta_{out} \tag{1-1}$$

Where γ is charge balance factor, $\eta_{S/T}$ is the ratio of radiative excitons (it is assumed as 1 for phosphorescence and 0.25 for fluorescence), q_{eff} is the quantum yield of the emitter and η_{out} is outcoupling efficiency. Studies for improving efficiencies of OLEDs focus on improving each parameter. Optimizing device structure for good charge balance, developing of phosphorescent OLEDs[2] and thermally assisted delayed fluorescence (TADF)[3] to increase the ratio of radiative excitons, synthesizing of the new emitter which has good photoluminescence quantum yield and developing an optical structure for extracting photon are such approaches.

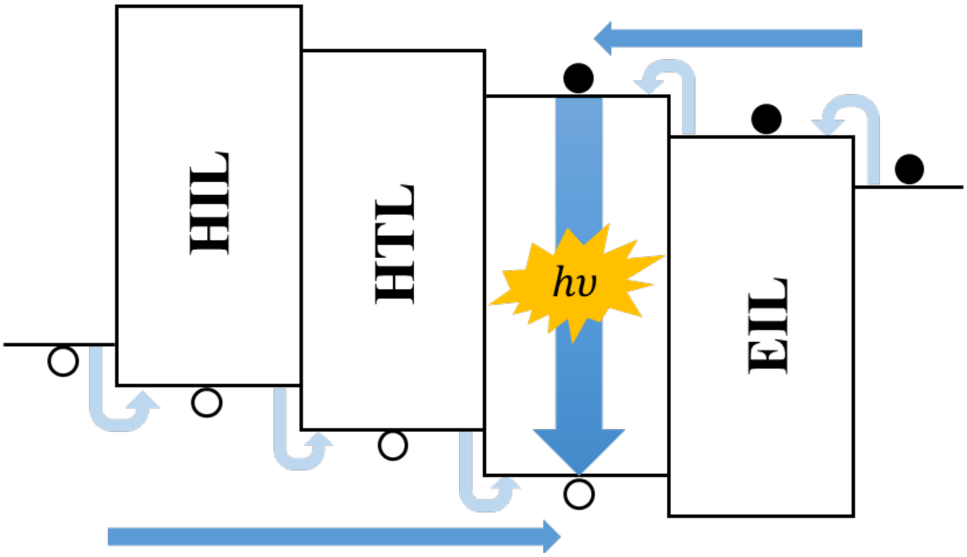

Figure 1.1 The structure and driving principle of typical OLEDs

1.2 Langevin recombination and Trap assisted recombination

There is two main recombination mechanism studied in the fields of the organic semiconductor. One is Langevin recombination[4] and the other is trap assisted recombination.[5] Langevin recombination also called bimolecular recombination, is recombination between the mobile hole and mobile electron. Origin of this behavior is Coulomb interaction between two particles. If thermal energy k_BT (0.026 eV at room temperature) of the particle is lower than Coulomb energy, they eventually capture each other. In this regards, the critical Coulombic capture radius can be defined,

$$r_c = \frac{q^2}{4\pi\varepsilon k_B T} \tag{1-2}$$

But the effect of this capture radius is canceled because recombination current from a hole to an electron is proportional to the field generated by hole ($\frac{q}{4\pi\varepsilon r^2}$) and recombining area generated by electron ($4\pi r^2$). Considering all this, rate of Langevin recombination is defined as equation (1-3)[4],

$$R_L = \frac{q}{\varepsilon}(\mu_n + \mu_p)np \tag{1-3}$$

where μ_n and μ_p are mobilities of electron and hole, respectively. The value of $\frac{q}{\varepsilon}(\mu_n + \mu_p)$ is often referred as Langevin recombination constant. As the mobility of the charge increases, chance to find opposite charge carrier also increases. Also, this rate is proportional to the density of each carrier.

The other mechanism is trap assisted recombination, also called as Shockley-Read-Hall recombination. This is the recombination between trapped charge and mobile charge with the opposite sign. In this case, trapped charge is immobile, so the rate of recombination is proportional to the mobility of mobile charge carrier. In case of hole trap system, this can be expressed as the following expression (equation (1-4)).

$$R_{pt} = \frac{q}{\varepsilon}\mu_n n p_t \tag{1-4}$$

Recombination mechanism plays a central role in the operation of optoelectronic devices. In OLEDs, recombination generates an exciton that produces a photon. With the presence of electron trap due to defect[6,7], trap assisted recombination is often considered as a loss mechanism in the polymer light emitting diodes.[8,9] But most of the OLEDs with high efficiencies are doped with the emitter in order to light the desired wavelength and to reduce loss due to concentration quenching. In this case, the trapped hole at the emitter also participates in the photon-generating process by forming exciton at the

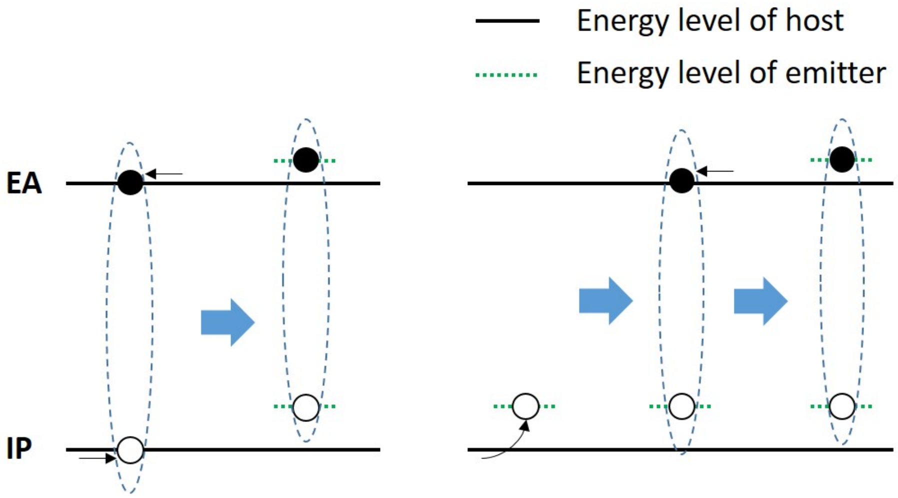

Figure 1.2 The competing recombination processes in dye-doped OLEDs : Langevin recombination (left) and trap assisted recombination (right).

emitter directly. Both mechanisms are used for phosphorescent dye-doped OLEDs because triplet exciton generated at the emitter also can be utilized. However, driving characteristics of the device can be varied with dominant recombination mechanism. Due to electric field formed by trapped charge, driving voltage of the devices increases compared to Langevin dominant system.[10] Also, in the case of triplet harvesting system using phosphorescent or TADF dye as a sensitizer and fluorescent dye as an emitter, trap assisted recombination is recommended in sensitizer, but not recommended in the emitter. Unlike sensitizers, fluorescent dye can't utilize triplet state for generating photons. So characteristics of devices and recombination mechanisms are closely related. Therefore, understanding of recombination mechanisms and factors affecting this phenomenon is important.

Recombination characteristics in the organic electronic devices can be characterized by experiments. First, ideality factor analysis based on Shockley diode equation[11] can be suggested.[12]

$$J = J_0\left[\exp\left(\frac{qV}{\eta kT}\right) - 1\right] \tag{1-5}$$

Where J_0 is saturation current density and η is ideality factor. This equation describes diffusion current of the diode, so only can be applied when the applied voltage is close to built-in potential (where diffusion current dominant). Ideality factor becomes 1 if there is only Langevin recombination mechanism through the devices (‘ideal (η=1)’ means there is no trap in the diode). By changing above equation the above equation in terms of η, ideality factor of the device from J-V characteristics can be calculated by the following expression,

$$\eta = \left(\frac{kT}{q} \frac{\partial \ln J}{\partial V} \right)^{-1} \tag{1-6}$$

For the Langevin dominant system, η is close to 1 and the trap dominant system, η is close to 2. For the application of this method, the device under test must show space charge limited characteristics. So injection into the device should be ohmic and high current density at diffusion current region is needed. additionally, minimization of leakage current is needed.[12]

Transient electroluminescence (EL) measurement also can be used to verify recombination mechanism in the OLEDs.[13-15] They are many causes of overshoot characteristics in transient EL including triplet-triplet annihilation[16,17] and degradation of injection layer.[14] However, in phosphorescent OLEDs, this overshoot characteristic is mainly attributed to trapped charge at the emitter because emitter forms trap site within the energy level of the host. In the measurement, a voltage pulse is applied to the device, then resulting electroluminescent characteristics is measured. Depending on the amount of charge accumulated at the emitter, overshoot characteristics of decay part increases with reverse bias at off-voltage.[18] The origin of this behavior is that detrapped charge is accelerated through reverse bias. However, overshoot at the decay part due to trapped charge can’t be observed if there is no energetic barrier for the accumulation of charge.[19] In addition to decay after off-voltage, overshoot can be also observed in the on-pulse region. This is due to the residual trapped charge at previous pulse.[19]

Above methods have some limitation for verifying recombination mechanism. Ideality factor can be only used in diffusion current region, and the device should ensure high carrier density in the devices so application of this method is limited. Also, for transient EL methods, its data should be judged based on the structure of the device and internal physical phenomena. Furthermore, for both methods show the tendency of device recombination, but it does not show how much it is. To remedy with this situation, calculation of Langevin recombination with electrical modeling can be suggested.[20]

$$P_L = \frac{\int R_L dx}{\int (R_L + R_{pt}) dx'} \tag{1-7}$$

Using above formula with charge density and mobility calculated with modeling, a portion of Langevin recombination, P_L, can be directly calculated. From the value of P_L, the dominance of certain recombination can be verified.

Also, by assuming virtual devices, the effect of various parameters on recombination mechanism can be tested.

1.3 Devices with Exciplex Forming Co-host System

Exciplex is an excited state formed between molecules of heterospecies. One electronically excited species M* may interact with other polar or polarizable ground state molecule N, forming stabilized charge-transfer state M*N.[21] Whereas for the ground state MN, there is no stabilization energy for this state, so these complexes dissociate rapidly. The emission characteristic of exciplex is therefore different from M* or N* state. Exciplex shows red shifted photoluminescent characteristics from consisting monomers due to stabilization energy.[22] Also, because two molecules act as donor and acceptor in exciplex state, there is little overlap between HOMO and LUMO orbital ($\left\langle \phi_D^* \middle| \phi_A \right\rangle$). So exchange energy ($J$) between singlet and triplet state is small which result in little energy gap between two states ($=2J$).[23] In fluorescence, triplet state is a non-radiative process but with small ΔE_{st}, thermal activation from triplet state to singlet state is possible. This is the same principle as thermally activated delayed fluorescent (TADF), which has been actively studied recently. Compared to Exciplex systems have the advantage of being able to make a combination of already known materials.

Recently, highly efficient OLEDs with exciplex host been reported. In phosphorescent OLEDs, doping phosphorescent dye in exciplex forming co-host have been reported the devices with EQEs over 30 %.[1,22,24-28] Also, these devices are reported with low driving voltage characteristics with high luminous efficiency. This is mainly attributed to low injection barrier from electrodes to emissive layer and balanced hole and electron mobility.[29] In addition to these factors, the dominance of Langevin recombination followed by energy transfer over direct trapping to dopant can be suggested. Because trapped charge induces an electric field in the device, which results in an increased driving voltage of the OLEDs.[10] In some researches report Langevin dominant characteristic of exciplex forming co-host system.[19,22] Also, there are approaches for utilizing exciplex system doped with fluorescent dye because enhancing color quality and lifetime of the OLEDs is other important issues. But EQE of this devices still limited (~ 15%) compared to phosphorescent OLEDs. Using high reverse intersystem crossing rate (RISC) in exciplex host, triplet exciton can be utilized. Using this strategy, 4 fold increase in IQE can be achieved. In this devices, charge trapping to fluorescent dye is an unfavorable phenomenon because generating excitons at emitter produces 1:3 ratio of singlet and triplet, so 75% of excited states can’t be utilized. So trapping at the emitter should be minimized. Given these situations, understanding recombination mechanism in the OLEDs is important to enhance driving characteristics and efficiencies of the OLEDs.

1.4 Outline of the thesis

We analyzed the factors that determine the recombination mechanism in the OLED comprehensively. To do this, the drift-diffusion modeling is introduced to analyze physical phenomena regarding on various parameters: energy level, mobility, trap depth and dipole moment of emitters.

The overview of drift-diffusion modeling and methods are explained in Chapter 2. First, Governing equations in drift-diffusion modeling are presented. Then physical phenomena considered in the model (especially, trapping kinetics and recombination mechanism), implementation of modeling (finite difference method) and calculation procedure of simulation (how to achieve steady state in the coupled differential equations) are explained in detail. In Chapter 3, the effect of the interlayer barrier, trap depth and mobility of the emissive layer on the recombination mechanism is studied. A virtual device that consists of a hole transporting material, an exciplex forming co-host and an electron transporting material is simulated to explain Langevin dominant characteristics of highly efficient exciplex system. With a variation of parameters, charge density distribution and corresponding Langevin and trap assisted recombination rates are calculated with the simulation. Through this study, we found that exciplex forming co-host system is a suitable platform to make Langevin dominant system. In Chapter 4, the effect of a new parameter, the dipole moment of the emitter on the recombination mechanism is studied. Considering trapping phenomenon as Coulomb interaction between a dipole and a charge, capture cross section of dopant depending on the dipole moment is calculated and introduced in the drift-diffusion modeling. As a result, dipole dependence of recombination mechanism is demonstrated. Correlation between dipole and recombination characteristics was also shown through experiments. Dopants with large dipole moment over 5 Debye (e.g., homoleptic Ir(III) dyes) induce large charge trapping on them, resulting in increased driving voltage and trap-assisted-recombination dominated emission. However, dyes with small dipole moment below 2 Debye (e.g., heteroleptic Ir(III) dyes) show much less trapping on them no matter what the magnitude of the trap depth is. We calculated the effect of trap depth and dipole moment on the portion of Langevin recombination. As a result, we found that dipole moment becomes dictating parameter when trap depth is > 0.25 eV.

Chapter 2. Electrical Modeling

2.1 Introduction

Depending on the scale of the model, electrical modeling can be categorized. The simplest one is equivalent circuit model commonly used in organic solar cells.[30] This model considers series resistance that includes the effect of the bulk resistance of material and contact resistance, and parallel resistance that includes the effect of the leakage currents. But this model is too simple It is too simple to deal with physical phenomena inside the devices. There are also analytical model which decribes field dependent space charge limited current density derived from Mott-Gurney law[31,32] or injection limited current density. Due to simplicity in the calculation, many models have been developed to narrow the gap with the actual device.[33,34] However, these models are only applicable to unipolar devices and can’t applicable to devices with multilayer structure. So the model describing the motion of the charge is needed.

There are more physically detailed models based on this approach. Microscopic model which is based on first principle approach is one of them.[35] It derives device characteristics from molecular property to transport property by calculating the molecular properties by density functional theory, the morphology by molecular dynamics simulations and the charge transport by Marcus theory. However, this approach is computationally demanding and can't be applied to the system of a few hundred nanometers, which is the typical thickness of OLED. There is also lattice Monte Carlo method based on Miller-Abrahams hopping theory.[36,37] This method implements disorder, percolation transport characteristics explicitly. However, assuming/fitting parameters such as localization length, lattice parameter and 'attempt to hop' frequency is inevitable to derive transport characteristics. As a remedy for problems in two methods, the coarse-grained model can be used.[35] This method considers morphology, site energy, reorganization energy and electrical coupling by introducing models describing each phenomenon, and each result is highly consistent with the results using the atomistic model.[35] Using each parameter as input parameters for kinetic Monte Carlo model, this can be applied to the larger system and have physical details.[38] However, this method still is time demanding and is used for parameterization of materials[35] or for analysis of physical phenomena in a single layer[39,40], but it is not utilized in large systems such as devices. Compared to these simulations which consume a lot of time and computer resources, drift-diffusion model can be an effective tool for modeling devices. There are still many studies based on drift-diffusion modeling nowadays.[29,41,42] Furthermore, The effect of the parameters on the characteristics of the device can be easily calculated compared to above simulations. Also, compared to the computational results of the physically detailed model, there is no significant difference if parameters are carefully selected.[35] From this advantage, we used drift-diffusion modeling to analyze the effect of dipole moment on recombination mechanism in the OLEDs studied in this thesis.

2.2 Governing Equations

Our model is based on a set of coupled differential equations. Acquiring solution from these equations, we can derive electric field, charge carrier density and current density of the device. The first differential equation is Poisson's equation.

$$\frac{\partial^2 V}{\partial x^2} = -\frac{q}{\varepsilon}\rho \tag{2-1}$$

Where V is the electrostatic potential, x is the distance from the anode, q is electrical charge of an electron, ε is the permittivity of the system and ρ is the space charge density. This is based on one of Maxwell's equation (Gauss's law), $\nabla \cdot E = \frac{\rho}{\varepsilon}$,. It describes the electric field of space charge density is depending on the sum of the contribution of charge carriers, $\rho = p + p_t - n - n_t + \ldots$.

The next equations are continuity equations. These equations describe transport/formation/extinction of charge at given point.

$$\frac{\partial J_p}{\partial x} + q\frac{\partial p}{\partial t} = -R \tag{2-2}$$

$$\frac{\partial J_n}{\partial x} - q\frac{\partial n}{\partial t} = -R \tag{2-3}$$

Where J_p and J_n are the current density of hole and electron, p and n are charge density of hole and electron and R is the recombination rate. J_p and J_n are expressed with transport equation. For diffusion, we used the classical Einstein relation ($D = \mu kT / e$).

$$J_p = q\mu_p pE - \mu_p k_B T \frac{\partial p}{\partial x} \tag{2-4}$$

$$J_n = q\mu_n nE + \mu_n k_B T \frac{\partial n}{\partial x} \tag{2-5}$$

For mobility of hole and electron, mobility measured with time-of-flight (TOF) method is used. Recombination of free hole and free electron is expressed using Langevin type recombination.

$$R_L = \frac{q}{\varepsilon}(\mu_n + \mu_p)np \tag{2-6}$$

In dye-doped OLED, the energy level dopants are located within the bandgap of host and the dopants act as trap site. In this case, trapping on the dopants should be additionally considered in the model. For hole trapping system with the trap depth of ΔE_t, trapping and detrapping of hole can be expressed as follows,

$$U_t = Sv_p \left[p(N_t - p_t) - p_t(N_{IP} - p)\exp\left(-\frac{\Delta E_t}{k_B T}\right)\right] \tag{2-7}$$

The first term in the square bracket describes trapping. This consists of capture cross section S, the velocity of holes v_p (=$\left|J_p\right| / qp$), p and the density of the trapping site $N_t - p_t$ which a hole can be trapped. The latter term describes detrapping. The detrapping consists of trapped hole density p_t, the

the density of empty site $N_{IP} - p$ which a trapped hole can escape to, and a Maxwell distribution term with the activation energy (i.e., trap depth).[43] The trapping phenomenon of electrons can also be expressed in the same form. Though we considered hole trapping system in this thesis, of course, the analysis can easily be extended to electron trapping or the trapping of both electrons and holes for other devices.

For the capture cross section S, this is first regarded as a colliding section of a molecule and its neighboring 4 molecules, assuming cubic lattice, it can be expressed as $S = 5 \times d_M^2$ where d_M is lattice constant.[43] Also, the trapping characteristics can be described as a Coulombic interaction between the free charge and μ_0 of the dopant. The trapping strength depends on the polarity of the dopant. The stronger μ_0 of the dopant is, the more readily it traps an encountered charge. We used the relationship between the S of a trap and the magnitude of the μ_0 derived by Belmont.[44] Assuming dipole located in polar coordinate with 0 degrees, potential formed by dipole depending on r and θ can be expressed as follows,

$$\phi = -\frac{q\mu_0 \cos\theta}{4\pi\varepsilon r^2} \tag{2-8}$$

If the thermal energy of a charge is lower than this value, they are eventually captured. With this regards, the critical radius can be derived,

$$-2kT = -\frac{q\mu_0 \cos\theta}{4\pi\varepsilon r_c^2} \tag{2-9}$$

Belmont calculated surface area of a sphere with r_c. If a charge passing by ‘touches’ this surfaces, they are captured.

$$S_0 = \int_0^{\frac{\pi}{2}} 2\pi \frac{q\mu_0}{8\pi\varepsilon kT} \frac{1}{2} (1+3\cos^2\theta)^{\frac{1}{2}} d(-\cos\theta) \tag{2-10}$$

The radius of this sphere is $(S_0 / 4\pi)^{1/2}$. So the area in which a passing charge can contact this sphere is denoted as $S = S_0 / 4$ which is a trap capture cross section of the dipole.

$$S = 1.4 \frac{q\mu_0}{32kT\varepsilon} \tag{2-11}$$

The following expression takes into account the repulsive forces that occur when the same sign is encountered which result in the reduced capture cross section.[44] Ignoring the contribution of the charge approaching the solid angle γ,

$$S = 0.7\left(1+\frac{\sqrt{3}}{4}\right)\frac{q\mu_0}{32kT\varepsilon} \tag{2-12}$$

This relationship describes the interaction between a charge and a dipole. In phosphorescent dye-doped OLEDs, emitter act as a trap. So this formula can be applied to the system.

In the presence of trapped charge, governing equations are modified. For example, trap-assisted recombination between the trapped hole and free electron should be considered.

$$R_{pt} = \frac{q}{\varepsilon}\mu_n n p_t \tag{2-13}$$

Also, reduction of the hole due to trapping, the contribution of the trapped hole in electrostatic potential also should be considered. To sum up, governing equations of hole trapping system are as follows,

$$\frac{\partial p}{\partial t} = -\frac{1}{q}\frac{\partial}{\partial x}\left(q\mu_p pE - \mu_p k_B T\frac{\partial p}{\partial x}\right) - R_L - U_t \tag{2-14}$$

$$\frac{\partial n}{\partial t} = \frac{1}{q}\frac{\partial}{\partial x}\left(q\mu_n nE + \mu_n k_B T\frac{\partial n}{\partial x}\right) - R_L - R_{pt} \tag{2-15}$$

$$U_t = Sv_p\left[p(N_t - p_t) - p_t(N_{IP} - p)\exp\left(-\frac{\Delta E_t}{k_B T}\right)\right] \tag{2-16}$$

$$\frac{\partial p_t}{\partial t} = U_t - R_{pt} \tag{2-17}$$

$$\frac{\partial^2 V}{\partial x^2} = -\frac{q}{\varepsilon}(p + p_t - n) \tag{2-18}$$

In OLED, hole transporting layer (HTL), emissive layer (EML) and electron transporting layer (ETL) are sandwiched between metallic electrodes, so interface between metal/organic layers occurs. In the modeling, thermionic injection is considered. In the case of metal/semiconductor interface, charge injection current can be expressed as follows[45],

$$J = \frac{em^*}{2\pi^2 h^3}(kT)^2 \exp\left(-\frac{\phi_B}{kT}\right)\exp f^{1/2}\left[\exp\left(\frac{eV}{kT}\right)-1\right] \qquad (2\text{-}19)$$

Where f is a unit-less parameter for the electric field, $f = eFr_c / k_B T$. For barrier for injection, ϕ_B, the difference in work function between metal and semiconductor is considered. Scattering of the injected carrier is not considered. In similar regards, current injection from metal to organic semiconductor is expressed as follows,[46]

$$J(f) = 16\pi\varepsilon\varepsilon_0 N_0 \mu\left(\frac{kT}{e}\right)^2 \exp\left(-\frac{\phi_B}{kT}\right)\exp(f^{1/2}) - n_0 e\mu\frac{E(x_c,0)}{4}\left(\frac{1}{\psi(f)^2} - f\right) \qquad (2\text{-}20)$$

where $\psi(f) = f^{-1} + f^{-1/2} - f^{-1}(1+2f^{1/2})^{1/2}$. The big difference from Richardson-Schottky model is that mobility of organic semiconductor is considered in the formula. This difference comes from the fact that Richardson model describes crystalline semiconductor. In the crystalline semiconductor, the electron is conducted with wavelike motion, freely propagates with ballistic motion in the solid-like vacuum.[47] However, this is not the case in the organic semiconductor. In organic solids, molecules are linked with week Van der Waals interaction rather than strong covalent bonds. Charge carrier moves with hopping transport rather than wavelike transport. In this case, movement of injecting carrier to the interface is another limiting factor. Also, the second term in the above equation is recombination current due to image charge.

2.3 Implementation of Drift-Diffusion Model

In our modeling, we used 1-Dimensional, equally spaced grid to simulate the devices (Figure 2.1).[43] Each grid corresponds to a monolayer with Δx spacing. This approach is valid because though hopping process of charge carriers occurs randomly with the biased direction, but a huge amount of carriers are involved and dimension of the monolayer is much larger than the thickness of the device, it allows description with averaged parameter implying overall characteristic (like mobility) in the simulation of device scale.

Depending on how the parameter is defined, each parameter is defined at a different location. Defining ITO/HIL interface as x = 0, each monolayers is placed at x = 0.5, 1.5, 2.5 … and so on. For each location, the hole density is defined as p^1, p^2, p^3 … and so on. However, for the electric field, it is defined at the interface when calculated through Poisson's equation. So F_{if}^1, F_{if}^2, F_{if}^3 … are defined at x = 1, 2, 3, … which are the interfaces between the monolayers. The electric field at the monolayer should be additionally considered because of drift term of current.

$$F^i = \frac{F_{if}^{i-1} + F_{if}^i}{2} \tag{2-21}$$

In addition to the electric field, current density given point is defined at the interfaces for the same reason.

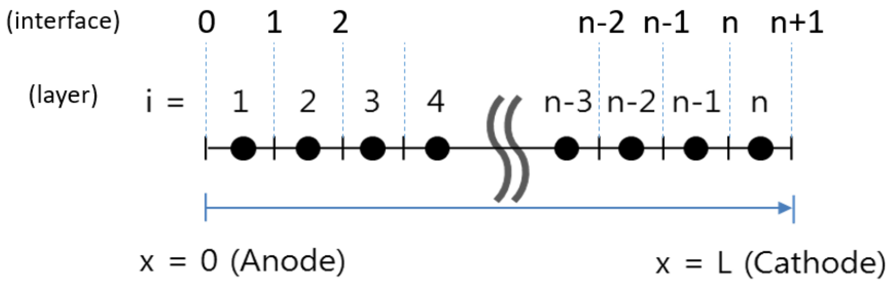

Figure 2.1 Discretization and indexing used in the model. Starting from the anode, index increases. The indexing number for interfaces and monolayer are indicated.

To derive a solution from Poisson's equation, we need boundary condition for the differential equation. Sum of the contribution of electric field equals the potential difference actually applied to the organic layer.

$$\int F dx = V - V_{bi} \tag{2-22}$$

We used our program written in MATLAB code. In this modeling, each change in the grid is defined along with the direction as well as the increment/decrement as ($\Delta p^{i\to i+1}$, $\Delta n^{i\to i+1} \ldots$).[43,48] In this method, components of holes or electrons moving to cathode or anode direction can be divided. Since only components moving to the barrier should be considered, this is important to calculate carrier component injecting into organic-organic interfaces. The continuity equations are divided according to the mechanism and direction of transport. Transport component from grid *i* to *i*+1 of hole can be described with velocity, grid spacing and carrier density,

$$\frac{\Delta p^{i\to i+1}}{\Delta t} = \frac{v^i}{\Delta x} p^i \tag{2-23}$$

Then the change of hole density by drift can be expressed by applying drift velocity $\mu_p^i F^i$ in the v^i. Drift current occurs along the direction of electric field, if the negative electric field is applied, $\Delta p_{drift}^{i\to i+1}$ becomes zero. (Instead, there would be a non-zero component of $\Delta p_{drift}^{i\to i-1}$.) For the diffusion current, the diffusion velocity described with diffusion coefficient is applied. The classical Einstein relation ($D = \mu kT / e$) is used for the diffusion coefficient. Different from drift current, diffusion current is non-directional. It occurs in all directions with respect to the density at a given point ($\Delta p_{diff}^{i \to i+1} = \Delta p_{diff}^{i \to i-1}$). Summing this, rate of change of hole can be expressed as

$$\frac{\Delta p_{drift}^{i \to i+1}}{\Delta t} = \begin{cases} \dfrac{\mu_p^i F^i}{\Delta x} p^i, & F^i > 0 \\ 0, & F^i \le 0 \end{cases} , \quad \frac{\Delta p_{drift}^{i \to i-1}}{\Delta t} = \begin{cases} 0, & F^i > 0 \\ -\dfrac{\mu_p^i F^i}{\Delta x} p^i, & F^i \le 0 \end{cases} \tag{2-24}$$

$$\frac{\Delta p_{diff}^{i \to i+1}}{\Delta t} = \frac{\Delta p_{diff}^{i \to i-1}}{\Delta t} = \frac{\mu_p k_B T}{e \Delta x^2} p^i \tag{2-25}$$

For the interface between organic layers, the additional exponential term is taken into account when carriers are passing through the barrier at the interface. Field-dependent barrier lowering effect is also considered.

$$\Delta p^{i \to i+1} = \Delta p_0{}^{i \to i+1} \exp\left(-\frac{\phi - e \Delta x F}{k_B T} \right) \tag{2-26}$$

The other terms like recombination, trapping already have forms of parameters defined in each grid, the rate of change is calculated simply.

$$\Delta p_{Langevin}^i = R^i = \frac{q}{\varepsilon} (\mu_n + \mu_p) n^i p^i \tag{2-27}$$

$$\Delta p_{p,trap}^i = R_{trap}^i = \frac{q}{\varepsilon} \mu_n n^i p_t^i \tag{2-28}$$

$$\Delta p_{trap}^i = S v_p^i p^i (N_t - p_t^i) \tag{2-29}$$

$$\Delta p^{i}_{detrap} = S v^{i}_{p} p^{i}_{t} (N_{HOMO} - p^{i}) \exp\left(-\frac{\Delta E_t}{k_B T} \right) \quad (2\text{-}30)$$

Considering all these terms, rate of change of hole at grid point *i* can be expressed as,

$$\begin{aligned} \Delta p^{i} &= -\Delta p^{i\to i+1}_{drift} - \Delta p^{i\to i-1}_{drift} - \Delta p^{i\to i+1}_{diff} - \Delta p^{i\to i-1}_{diff} \\ &\quad + \Delta p^{i+1\to i}_{drift} + \Delta p^{i-1\to i}_{drift} + \Delta p^{i+1\to i}_{diff} + \Delta p^{i-1\to i}_{diff} \\ &\quad - \Delta p^{i}_{Langevin} - \Delta p^{i}_{p,trap} - \Delta p^{i}_{trap} - \Delta p^{i}_{detrap} \end{aligned} \quad (2\text{-}31)$$

If grid point *i* is positioned next to electrode (i.e. anode or cathode), an additional term of the charge injection is also considered. In this case, the injected current is converted to the amount of injected charge density per second. Also at the injection contact, the contribution from thermionic injection current should be considered. In this case, the current was converted to the number of charges and added to the rate of change term.

Current density contributed by hole and electron can be expressed as follows,

$$J^{i}_{p} = e\left(\frac{\Delta p^{i\to i+1}}{\Delta t} - \frac{\Delta p^{i+1\to i}}{\Delta t} \right), \quad J^{i}_{n} = -e\left(\frac{\Delta n^{i\to i+1}}{\Delta t} - \frac{\Delta n^{i+1\to i}}{\Delta t} \right) \quad (2\text{-}32)$$

So the overall current density can be calculated by,

$$J^{i}_{p} = e\left(\frac{\Delta p^{i\to i+1}}{\Delta t} - \frac{\Delta p^{i+1\to i}}{\Delta t} - \frac{\Delta n^{i\to i+1}}{\Delta t} + \frac{\Delta n^{i+1\to i}}{\Delta t} \right) \quad (2\text{-}33)$$

The total current is the sum of hole and electron current, $J^{i}_{sum} = J^{i}_{p} + J^{i}_{n}$.

Flowchart of modeling is shown in Figure 2.2. This scheme continuously calculates new variables of states until a steady-state solution is achieved. Determination of steady state can be done by several conditions. First, whether the rate of change of variable at given time is under the threshold value. For example,

$$\left.\frac{\partial p}{\partial t}\right/ p < \delta \, , \quad \left.\frac{\partial n}{\partial t}\right/ n < \delta \qquad \text{(2-34)}$$

where δ means the size of error allowed in the model. Also, if displacement current due to change of electric field with time disappears, this also can be considered as a steady-state condition.

$$\varepsilon \frac{\partial F}{\partial t} \sim 0 \, , \quad J_{dis} / J_{sum} < \delta \qquad \text{(2-35)}$$

We checked both conditions for determining the steady state for the simulation.

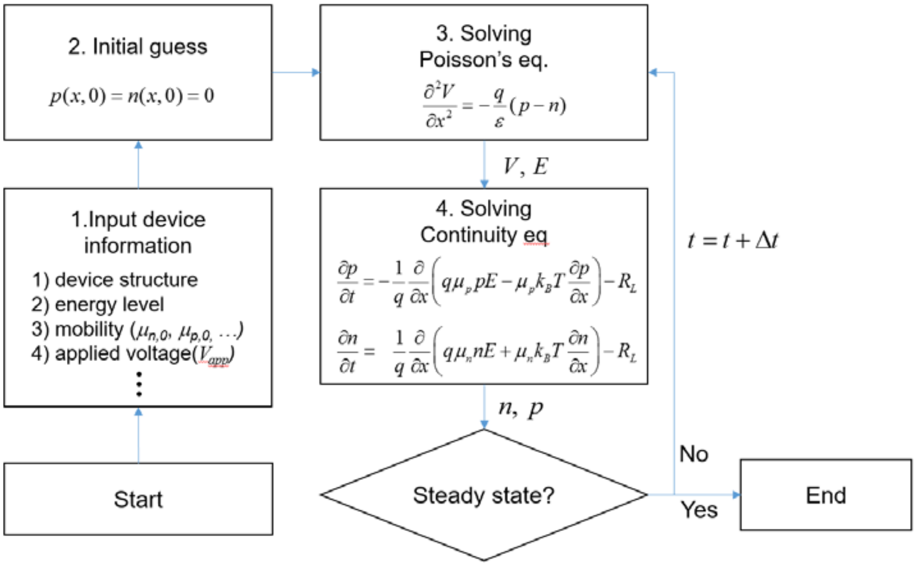

Figure 2.2 Flow chart for the drift-diffusion modeling. It is calculated repeatedly until steady state is obtained

Chapter 3. Factors Affecting the Recombination Mechanism in Dye-doped Organic Light Emitting Diodes

3.1 Introduction

The recombination of the injected or generated charge carriers in organic photonic devices such as organic light emitting diodes (OLEDs), organic photovoltaics, and organic lasers is one of the main key factors determining the efficiency, driving characteristics and lifetime of the devices. So understanding recombination mechanism in the organic semiconductor devices is important. The recombination process can be classified into two different mechanisms. One is trap-assisted recombination (TAR) between a trapped charge and the opposite free (or trapped) charge carrier. The other is Langevin recombination (LR) between a free electron and hole. These two mechanisms are mutually competitive under the operation of the phosphorescent, fluorescent, or thermally activated delayed fluorescent dye-doped OLEDs. Trap assisted recombination process in the OLEDs generally causes much higher accumulated charge carriers in the dopants state, where the ionization potential

(IP) or electron affinity (EA) of the dopants are within the bandgap of the host layer[18,49-55], whereas LR attributes to less trapped charge carriers in the OLEDs under the external bias. The accumulated polarons in the dopant state of the OLEDs potentially hinders the effective mobility of the injected charge carriers and annihilates the generated excitons as well as induces unnecessary local-field in the OLEDs during the operation. Therefore, LR is preferred against trap assisted recombination for high-performance OLEDs[19,22]. However, few fundamental understandings have been studied on determining the dominant mechanism between them during the electrical operation[19,56] and less information have been reported which parameters are important to promote LR and to demote trap assisted recombination.

Although there are lots of organic materials depending on molecule backbone and a functional group, study about the effect of a certain parameter is difficult. It is still hard to find material with a suitable parameter. Also, Even reported values of energy level and mobility are different because of disordered nature of organic semiconductor, parameters like energy level and mobility are not well characterized. So it is difficult to design experiments to see the effect of certain parameters. In this chapter, we are gonna present effect of parameters on recombination mechanism in the OLED based on the drift-diffusion model. The model contains physical description including injection, transport and recombination this approaches are not yet predictive, but can be used to explain the effect of parameters. In this study, we studied the effect of the energy level of the transport layer, trap depth and mobility of emission layer on recombination mechanism. Through this, it would be helpful to design and fabricate devices with desired recombination characteristics.

3.2 Experimental

In the simulation, the virtual device with symmetric structure is modeled. This device consists of an anode, a hole transporting material (HTM), an emissive layer (EML), an electron transporting material (ETM) and a cathode which is the typical structure of OLEDs.(Figure 3.1) The thickness of each layer is 40 nm/30 nm/40 nm. EML consists of the mixture of between HTM and ETM and forms exciplex. So excited state can be formed without additional energy to form an exciton. Also, EML is considered as an effective medium which has EA of ETM and IP of HTM. Mobilities of each layer used in the model are shown in Table 3.1. Injection barriers are assumed to be 0.3 eV for both injection barriers which is close to ohmic characteristics. The relative dielectric constant is 3.5 which is a typical value for organic materials. Also, room temperature (298 K) is assumed in the modeling.

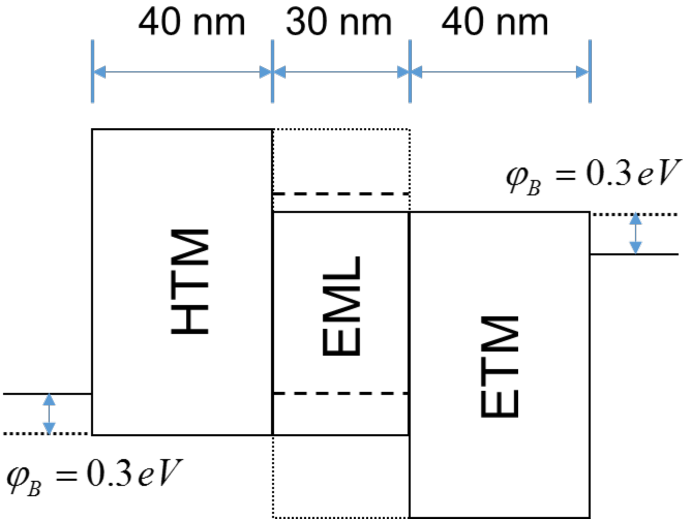

Figure 3.1 Device structure of virtual device studied with the drift-diffusion model

Table 2.1 Mobility values used in the drift-diffusion model

Material	μ_p [cm^2/Vs]	γ_p [cm$^{1/2}$/V$^{1/2}$]	μ_p [cm^2/Vs]	γ_p [cm$^{1/2}$/V$^{1/2}$]
HTM	1.0×10^{-6}	2.0×10^{-3}	1.0×10^{-6}	2.0×10^{-3}
ETM	1.0×10^{-6}	2.0×10^{-3}	1.0×10^{-6}	2.0×10^{-3}
EML	1.0×10^{-7}	2.0×10^{-3}	1.0×10^{-7}	2.0×10^{-3}

3.3 Result and discussion

We studied how interlayer barrier (ϕ_{adj}), trap depth (ΔE_t) and mobility of EML (μ_{EML}) influence on recombination mechanism in the devices. We calculated the distribution of hole, trapped hole and electron with the drift-diffusion model at 3 V and compared them depending on the variables.

First, the effect of ϕ_{adj} on the device is examined. By varying EA of HTM and IP of ETM, interlayer that is formed with EML is changed as 0, 0.05, 0.10, 0.15 and 0.20 eV. Charge carrier distribution depending on ϕ_{adj} is shown in Figure 3.2 (a). As ϕ_{adj} increases, accumulation of charge at interface also increases because ϕ_{adj} acts as an energetic barrier for the carriers from EML moving to the opposite side. As a result, charge carrier density at the EML increases, thus LR rate also increases (Figure 3.2 (b)).

Effect of μ_{EML} is also examined. μ_{EML} is varied as 10^{-9}, 10^{-8}, 10^{-7} and 10^{-6} cm^2/Vs. HTM and ETM have higher mobility than EML. This is reasonable situation because EML is the blend structure of HTM and ETM, holes or electrons are transported through HTM or ETM in EML but their average hopping distance is elongated. For the same reason, the mobility of

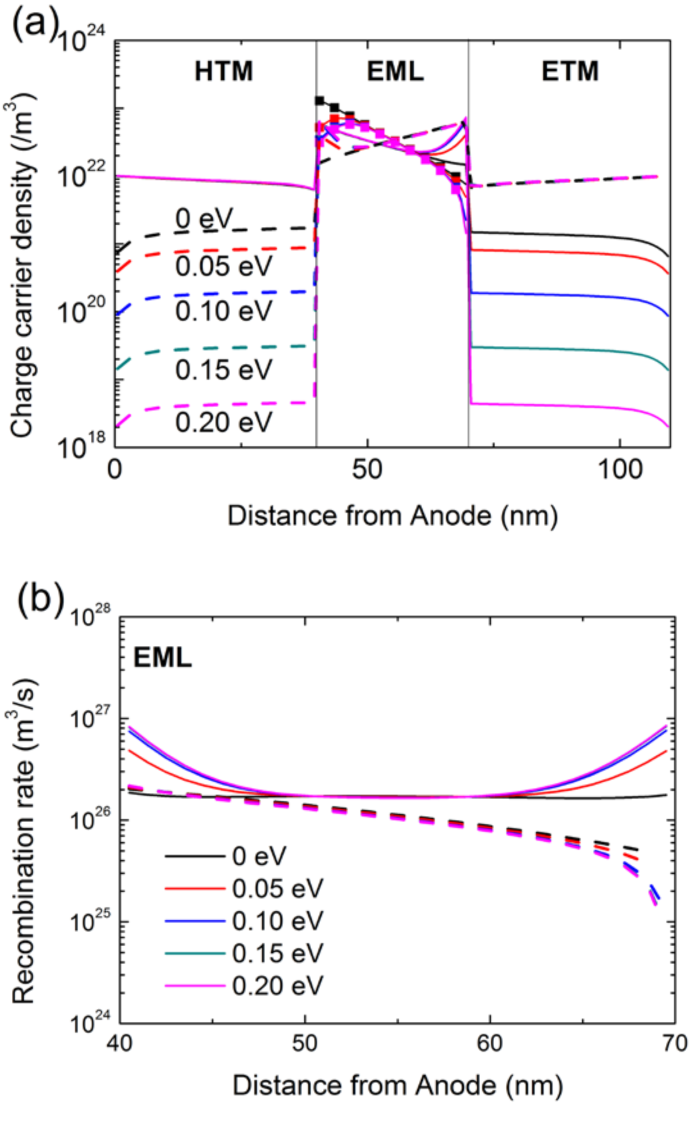

Figure 3.2 (a) charge carrier distribution (solid : hole, dashed : electron, symbol : trapped hole) and (b) rate of recombination (solid : Langevin, dashed : trap assisted recombination) depending on ϕ_{adj} = 0, 0.05, 0.10, 0.15, 0.20 eV.

TCTA:B3PYMPM is less than TCTA for hole and B3PYMPM for electron as shown in Chapter 4. For distribution of charge carrier, accumulation of charge at EML is increased as μ_{EML} decreases (Figure 3.3 (a)). This is due to the mobility difference between HTM and ETM. The larger the mobility gap, the more static the charge is near the interface. Note that density of trapped hole increases but the rate of trap assisted recombination decreases with decreasing of mobility (Figure 3.3 (b)). This is because mobility is also involved in the rate of trap-assisted recombination ($R_{pt} = \frac{q}{\varepsilon}\mu_n n p_t$). As a result, the portion of LR increases with decreasing μ_{EML}.

Finally, the effect of ΔE_t is examined. We changed ΔE_t as 0.1, 0.2, 0.3 and 0.4 eV. With increasing ΔE_t, the density of trapped hole increases because activation energy for detrapping is increased with ΔE_t (Figure 3.4 (a)). Note that there is no change for ΔE_t of 0.3 and 0.4 eV. This is because both values are well above the thermal energy of charge carrier (>> kT), detrapping is almost impossible for both ΔE_t. The density of trapped hole density is determined by trapping and trap assisted recombination with electron. As a result, the rate of trap assisted recombination increases with ΔE_t increases,

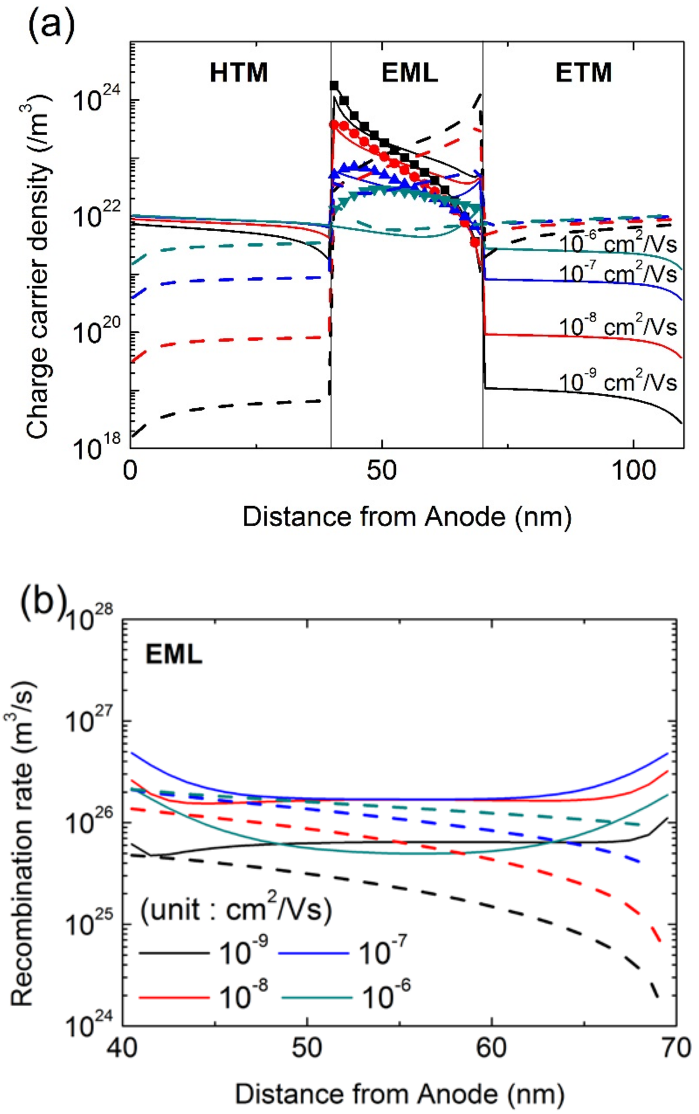

Figure 3.3 (a) charge carrier distribution (solid : hole, dashed : electron, symbol : trapped hole) and (b) rate of recombination (solid : Langevin, dashed : trap assisted recombination) depending on μ_{EML} = 10^{-9}, 10^{-8}, 10^{-7}, 10^{-6} cm^2/Vs

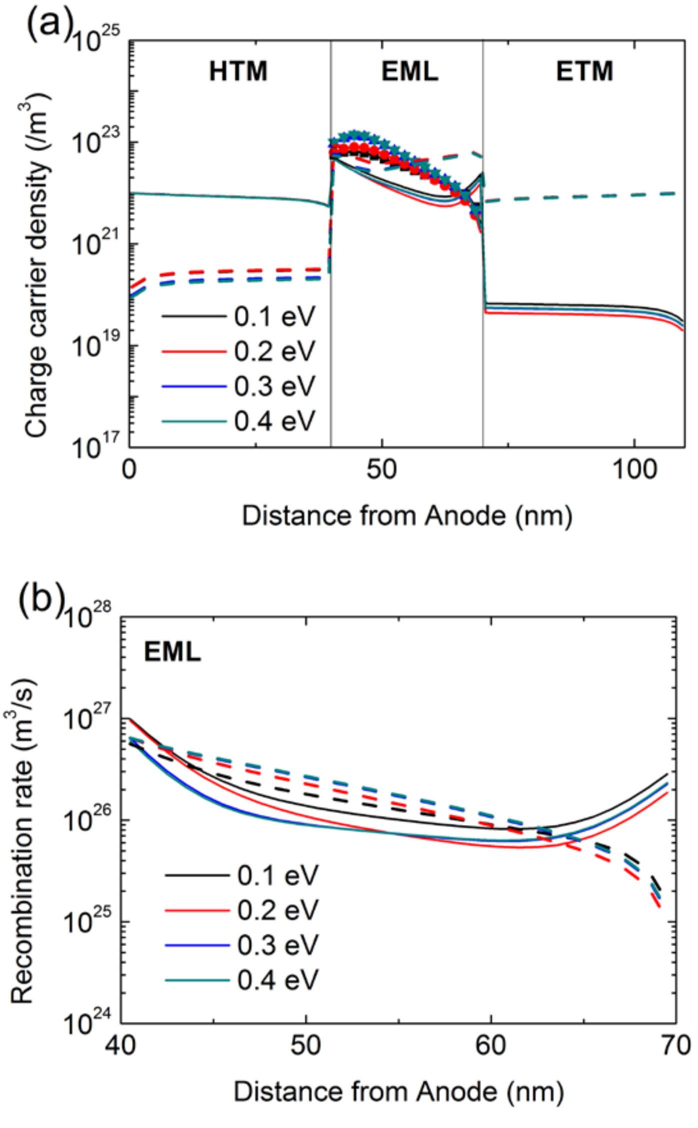

Figure 3.4 (a) charge carrier distribution (solid : hole, dashed : electron, symbol : trapped hole) and (b) rate of recombination (solid : Langevin, dashed : trap assisted recombination) depending on ΔE_t = 0.1, 0.2, 0.3, 0.4 eV

but saturates over 0.3 eV of ΔE_t .

Effect of ϕ_{adj} , μ_{EML} and ΔE_t on the distribution of charge carrier and recombination rates are shown. However, the effect of each parameter on recombination can be directly shown by calculating the portion of LR (P_L) over total recombination mechanism in the EML.[20]

$$P_L = \frac{\int R_L dx}{\int (R_L + R_{pt}) dx'} \tag{3-1}$$

With this formula, the dominance of certain recombination in the devices can be characterized with a single parameter by integrating recombination rate over EML. We plotted P_L against μ_{EML} (Figure 3.5) and ΔE_t (Figure 3.6) depending on ϕ_{adj} and μ_{EML} , but the mobility at the point of increasing is different. This is because both parameters have an effect on P_L by increasing charge density at the EML. Also, there is a maximum in P_L increase due to a decrease of μ_{EML} and an increase of ϕ_{adj} . Note saturation effect as shown in Figure 3.6. The P_L value to be saturated depends on the μ_{EML} . This is because the density of trapped hole is determined by trapping and rate of both mechanisms are related to μ_{EML} .

We studied virtual devices with drift-diffusion modeling, the structure of the devices (HTM/EML/ETM) is a common structure in the exciplex forming co-

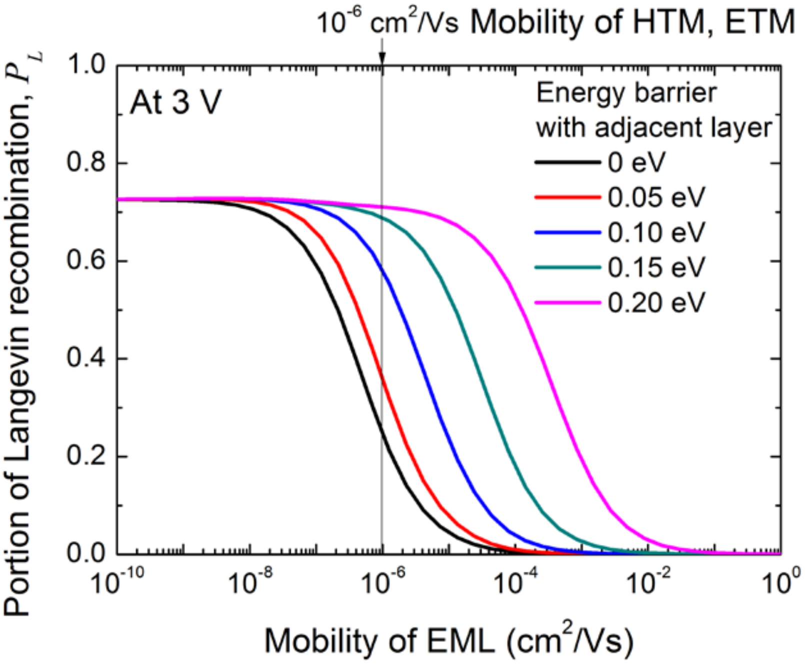

Figure 3.5 The portion of Langevin recombination (P_L) depending on μ_{EML} and ϕ_{adj}

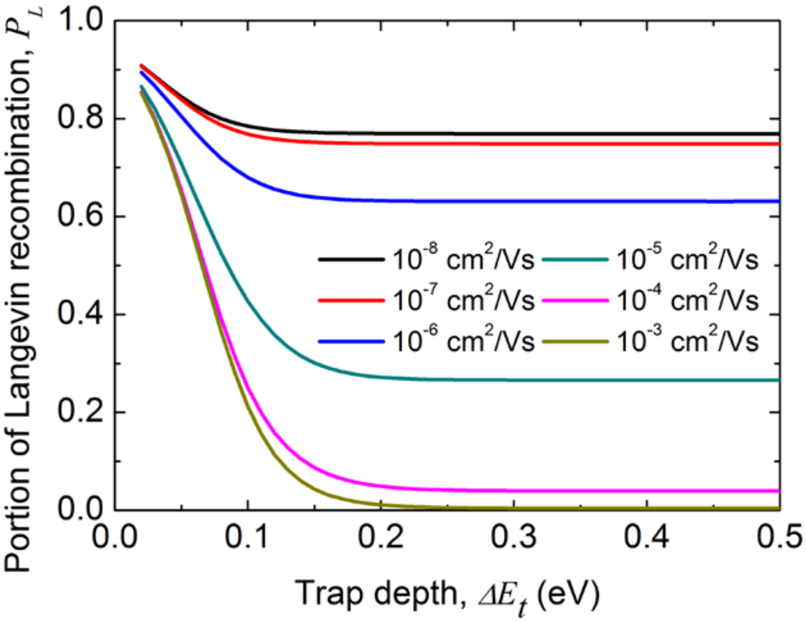

Figure 3.6 The portion of Langevin recombination (P_L) depending on μ_{EML} and ΔE_t

host system. Through modeling, we found that characteristics of this system (ϕ_{adj} with HTM and ETM, low μ_{EML}) are favorable for Langevin dominant system. So even with deep ΔE_t, fabrication of Langevin dominant system is possible. Also, by adjusting the ΔE_t through the dopant's energy level, it is possible to control recombination mechanism in limited situations. Through this study, we found that exciplex forming co-host system is a suitable platform to make Langevin dominant system.

3.4 Conclusion

The effect of ϕ_{adj}, μ_{EML} and ΔE_t on recombination mechanism is studied in the HTM/EML/ETM system which is the typical structure of exciplex forming co-host system. With drift-diffusion modeling, the effect of each parameter is calculated. As ϕ_{adj} increases, holes or electrons are accumulated at the EML/ETM or HTM/EML interface. This increases P_L through an increase in LR rate. Also, charge accumulation at EML also increases with decreasing μ_{EML} due to mobility gap between HTM and ETM. In spite of increased trapped hole density, the rate of trap assisted recombination is low due to decreased mobility, this also increases P_L. Different from other parameters, ΔE_t is directly related to trapped hole density by affecting detrapping characteristics. This effect is saturated when ΔE_t is over ~ 0.3 eV. Corresponding all this result to the exciplex system, we found that this system is easy to become LR dominant because it has lower mobility in the EML than HTM and ETM, and there always are barriers between EML and adjacent layers.

Chapter 4. Unveiling the Role of Dopant Polarity on the Recombination and Performance of Organic Light-Emitting Diodes

4.1 Introduction

The recombination of charges refers to a process whereby an electron and a hole are being annihilated and giving off energy. This process produces photons in organic light emitting diodes (OLEDs), but it is a loss mechanism that should be avoided in organic photovoltaics. Therefore, the recombination of charges is an important process in photonic devices, because the process influences the device characteristics such as the driving voltage, efficiency and lifetime. There are two possible recombination processes in dye doped organic semiconductors: Langevin recombination (LR) between a free electron and a free hole, and trap-assisted recombination (TAR) between a trapped charge and an opposite free charge.

Trapping in the dopant is known to affect the recombination mechanism in OLEDs.[12] Trap depth (ΔE_t) is considered as the major parameter affecting this trapping phenomenon.[57,58] Therefore, trap-assisted recombination is known as the dominant mechanism in phosphorescent dye-doped OLEDs (PhOLEDs) because the energy levels of the dopants are located deep compared with the host energy levels with large ΔE_t and the dopants act as trap sites.[18,49-55,59] In contrast, there have been reports that some PhOLEDs with deep trap depths have LR-dominant characteristics[10,19,22,60-62] which cannot be explained based on ΔE_t.[63]

Here, we report that the stationary dipole moment (μ_0) rather than ΔE_t of the dopant is a major factor influencing the trapping behavior and the recombination mechanism in dye-doped OLEDs. Our experimental results showed that homoleptic Ir-complexes possessing large μ_0 showed trapping-dominant characteristics exhibiting large driving voltage and TAR dominant characteristics, whereas heteroleptic Ir-complexes with small μ_0 lead to low charge trapping even with large ΔE_t, resulting in low driving voltage and LR dominant characteristics. Dopants with larger μ_0 can readily trap charges with stronger Coulomb attraction, which in turn boosts trap-induced characteristics. In addition, drift-diffusion model combined with dipole trap theory was used to investigate how the μ_0 of the dopants affects the recombination mechanism and the device characteristics. The results show that

μ_0 of the dopants plays a dominant role in recombination rather than ΔE_t if ΔE_t is larger than 0.25 eV where any de-trapping effect becomes negligible. Dopants with large μ_0 over 5 Debye (for instance, homoleptic Ir(III) dyes) induce trap assisted recombination. In contrast, dyes with small μ_0 below 2 Debye (e.g., heteroleptic Ir(III) dyes) much less trapping on them resulting in LR even though ΔE_t is much larger than 0.25 eV.

4.2 Experiments

Device Fabrication: Prior to the deposition, the ITO glass were exposed to UV-ozone flux (15 min) followed by cleaning with deionized water and boiling IPA. Devices were fabricated under ultralow vacuum (5×10^{-7} Torr). All layers were evaporated thermally and deposited on pre-cleaned patterned ITO electrodes on glass substrates without breaking the vacuum. The active area of the devices is 2×2 mm^2. All devices were encapsulated with glass lids using an ultraviolet curing resin.

Device Characterization: J-V-L characteristics were measured with a voltage-source-measure unit (Keithley 237) and a SpectraScan PR650 (Photo Research). Transient EL data were obtained using a pulse generator (Agilent 8114A) and a spectrometer (SpectraPro-300i) connected to a photomultiplier tube (Acton Research, PD-438). Mobilities were measured with time-of-flight measurement equipment (Optel, TOF-401). Energy levels were measured with cyclic voltammetry (VSP Princeton Applied Research) and UV-vis-absorption equipment (Agilent, Cary 5000)

4.3 Device Characteristics (*J*-*V*-*L*, transient EL)

Figure 4.1 shows the schematic diagram of the device structure along with the energy levels of the organic layers. The detailed device structure is ITO(70 nm)/TAPC(75 nm)/TCTA(10 nm)/TCTA:B3PYMPM:Ir dopant(1:1 molar ratio and 8 wt%, 30 nm)/B3PYMPM(45 nm)/LiF(0.7 nm)/Al(100 nm), where TAPC, TCTA and B3PYMPM represent di-[4-(N,N-ditolyl-amino)-phenyl]cyclohexane, 4,4′,4″-Tris(carbazol-9-yl)triphenylamine and bis-4,6-(3,5-di-3-pyridylphenyl)-2-methylpyrimidine, respectively. The device has an exciplex-forming mixed host to provide a good charge balance and a low injection barrier.[1,22,24] The electron affinity (EA) of B3PYMPM and the ionization potential (IP) of TCTA work as the quasi-EA and -IP levels of the emitting layer. The device structures were the same for all the dopants to minimize the effect of parameters other than dopant properties. We selected three heteroleptic [$Ir(ppy)_2(acac)$, $Ir(mpp)_2(acac)$, and $Ir(ppy)_2(tmd)$] and three homoleptic Ir(III) complexes [$Ir(ppy)_3$, $Ir(mppy)_3$], and $Ir(chpy)_3$] whose chemical structures and energy levels are shown in Figures 4.2 and 4.3, respectively. The IP of the materials were determined using the cyclic voltammetry (CV) measurements. The IP of NPB (-5.4 eV) was used as the reference in the measurements. Then EA of the materials are

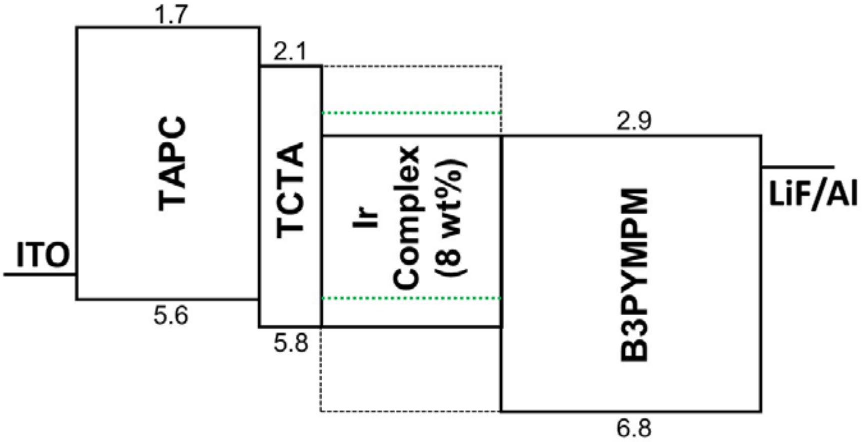

Figure 4.1 Schematic diagram of device structure with IP and EA of the consisting layers of PhOLEDs

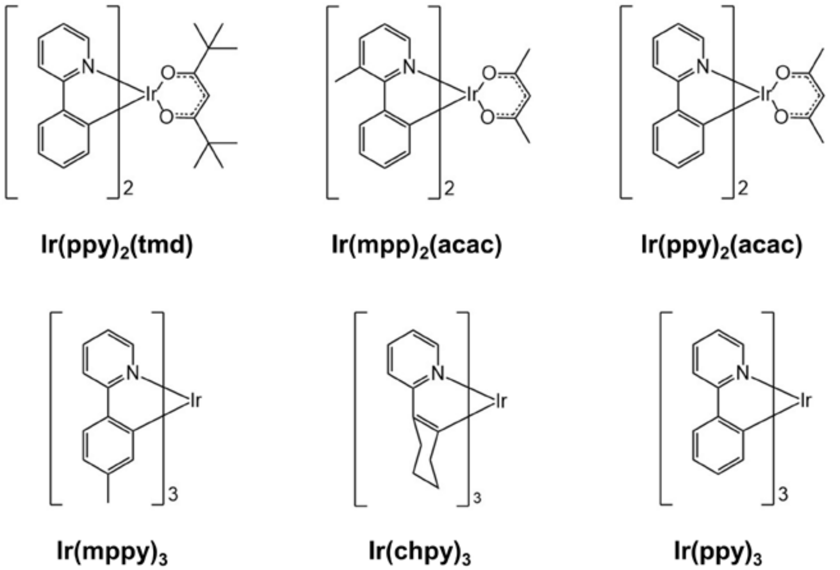

Figure 4.2 Chemical structures of Ir complexes used as emitters in the device

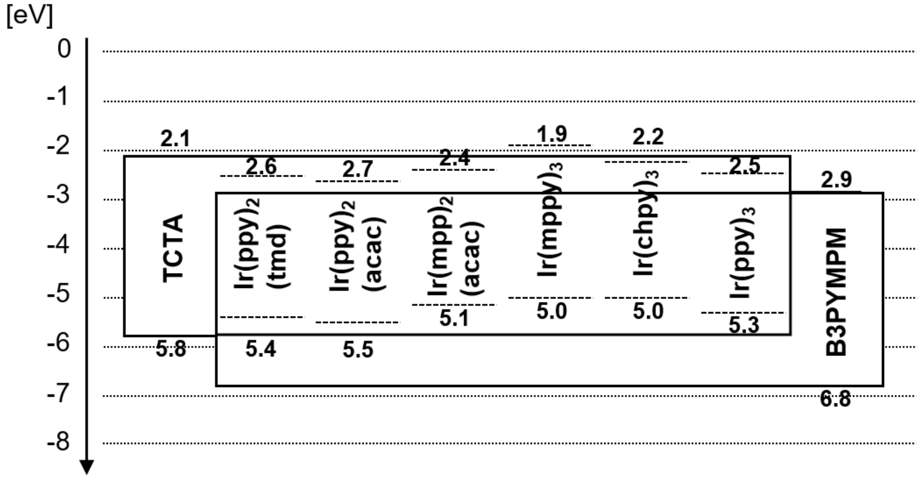

Figure 4.3 IP/EA of emitters used in the devices, energies are labeled in eV

estimated by the addition of the optical gaps and assumed binding energy of exciton (~ 0.3 eV) to the IP's. The dopants have higher EA's than B3PYMPM and higher IP's than TCTA. Thus, they are expected to behave as hole traps. Calculated μ_0 of the dopants, capture cross section S and ΔE_t defined as the difference between the IP level of TCTA and that of the dopants are summarized in Table 4.1. It is known that trapping characteristics of dopant increases with ΔE_t gets large, acting as a deep trap.[50,58] μ_0 of the Ir-dopants were calculated with the density functional theory using the program Gaussian09.[64] Geometry optimization was performed using the B3LYP exchange-correlation functional, the LANL2DZ basis set for the Ir atom, and the 6-311G(d) basis set for all other atoms. μ_0 of the dopants are largely different between the heteroleptic and homoleptic dyes. The homoleptic Ir(III) complexes have μ_0 larger than 5 Debye and the heteroleptic Ir(III) complexes have μ_0 smaller than 2 Debye. The symmetry of the N-heterocycles exhibiting an electron-deficient region determines the μ_0 of the Ir complexes.[28] The facial-type homoleptic Ir complexes had three identical main ligands contributing to μ_0 along the C3 axis. In contrast, the μ_0 of heteroleptic Ir complexes is smaller than that of homoleptic Ir complexes because two N-heterocycles are placed on opposite sides with respect to the

Table 4.1 Trap depths (ΔE_t **),** static dipole moments (μ_0 **)**, capture radii and S of Ir complexes.

Heteroleptic dopants	Ir(ppy)$_2$(tmd)	Ir(mpp)$_2$(acac)	Ir(ppy)$_2$(acac)
ΔE_t [eV]	0.4	0.7	0.3
μ_0 [Debye]	1.40	1.64	1.83
Capture radius [nm]	0.21	0.26	0.28
Cross section [nm^2]	0.18	0.21	0.24
Homoleptic dopants	Ir(mppy)$_3$	Ir(chpy)$_3$	Ir(ppy)$_3$
ΔE_t [eV]	0.8	0.8	0.5
μ_0 [Debye]	5.38	6.18	6.36
Capture radius [nm]	0.47	0.51	0.51
Cross section [nm^2]	0.70	0.81	0.83

iridium atom, which cancels out to reduce the total μ_0.

Figure 4.4 (a)-(b) show the current density-voltage (*J–V*) and luminance-voltage (*L–V*) characteristics of the devices, respectively, for the six different dopants. The three OLEDs doped with the heteroleptic dopants show almost similar *J–V* characteristics. However, the other devices doped with the homoleptic dopants exhibited lower current densities than those with heteroleptic dopants at a specific voltage and their *J–V* characteristics are different from each other. Also, the turn-on voltages of the devices doped with the homoleptic dopants are higher than the heteroleptic dopants. Figure 4.5 shows external quantum efficiency (EQE) against the luminance of the devices. The maximum EQEs were high with 32.3%, 30.2%, 30.0%, 25.8%, 22.4% and 23.2% for $Ir(ppy)_2(tmd)$, $Ir(mpp)_2(acac)$, $Ir(ppy)_2(acac)$, $Ir(ppy)_3$, $Ir(mppy)_3$, and $Ir(chpy)_3$, respectively. These experimental values very well match with maximum achievable EQEs simulated by the classical dipole model considering photoluminescence quantum yield and horizontal dipole ratio (32.0%, 30.3%, 30.5%, 25.9%, 22.6% and 22.3%, respectively).[1,65,66] These results show that the devices are well optimized electrically and optically with excellent hole and electron balance. Figure 4.6 shows the comparison of the operating voltages among the devices. The difference of the driving voltages

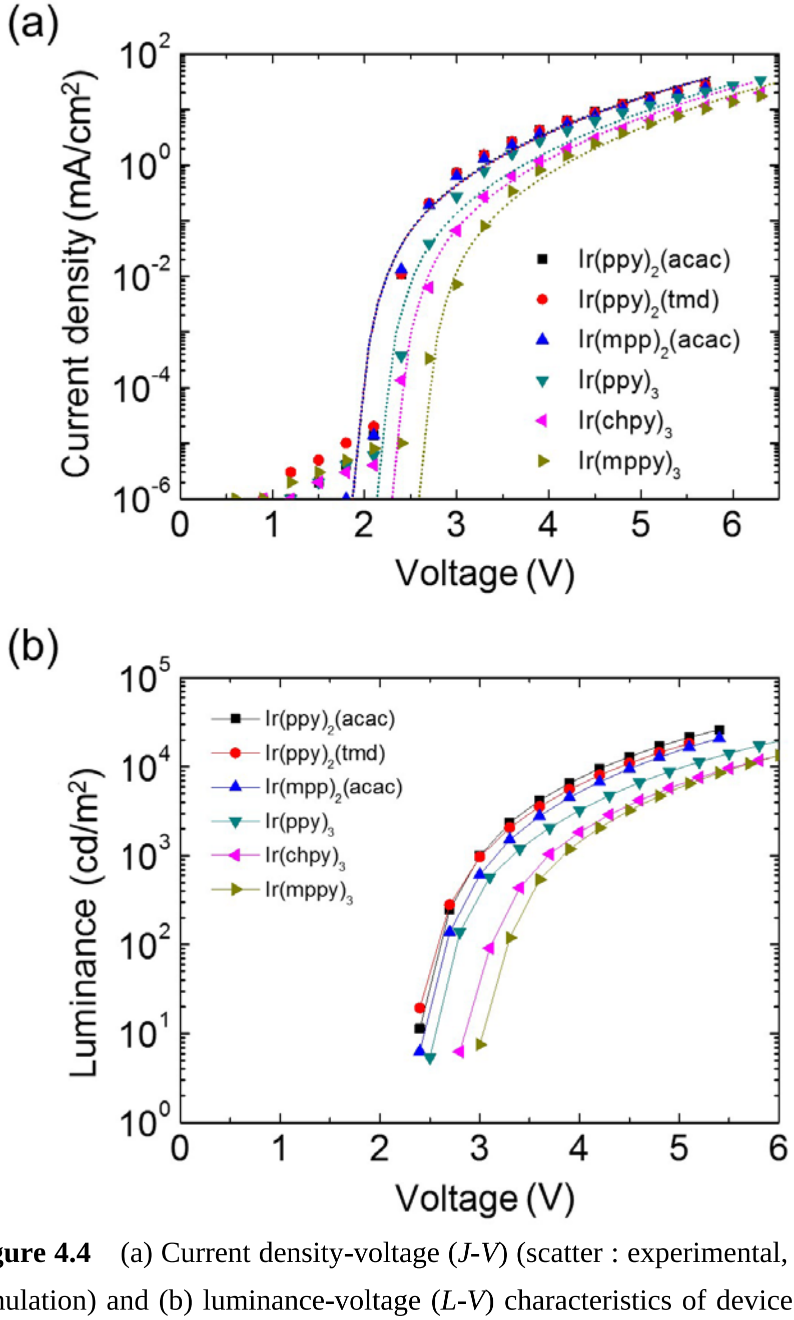

Figure 4.4 (a) Current density-voltage (*J*-*V*) (scatter : experimental, dotted : simulation) and (b) luminance-voltage (*L*-*V*) characteristics of devices doped with various phosphorescent dyes.

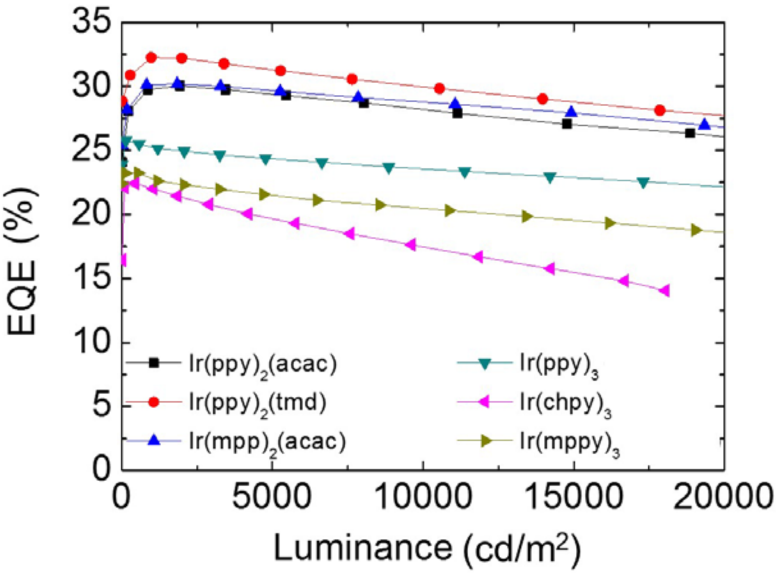

Figure 4.5 External quantum efficiencies (EQEs) against the current density of OLEDs doped with various phosphorescent dyes.

(ΔV) of the devices from the $Ir(ppy)_2(acac)$ doped device are plotted against the luminance of the devices. The operating voltage of the devices shows very different behaviors depending on the type of the dopants. Homoleptic dyes resulted in higher ΔV than the heteroleptic dyes and the ΔV of the devices. For instance, ΔV's are over 0.4 V at 20 mA/cm^2 for the homoleptic dyes, whereas the values of the device with the heteroleptic dyes below 0.25 V. The difference in *J–V–L* characteristics between the homoleptic and heteroleptic dopants may be due to the degree of trapping, because the charge trapping on the dopant lowers *J* by reducing carrier mobility in the emitting layer.[10,51,54,67,68] It is especially interesting to note that $Ir(mpp)_2acac$ possessing a similar IP or ΔE_t as $Ir(mppy)_3$ and $Ir(chpy)_3$ do show very different *J–V* characteristics as the homoleptic dyes, but show similar *J–V* characteristics as the heteroleptic dyes.

The transient EL of the devices clearly confirmed the charge trapping in the homoleptic Ir(III) complex-doped devices (Figure 4.7). None of the heteroleptic dopant-based devices exhibited any overshoot in the decay curves under reverse bias after turn-off of the electrical pulse. In contrast, all the homoleptic dopant-based devices exhibited either overshoots or initial delay under reverse bias, although the degree of overshoot or initial delays differed with different dopants. This overshoot or initial delay can be interpreted based

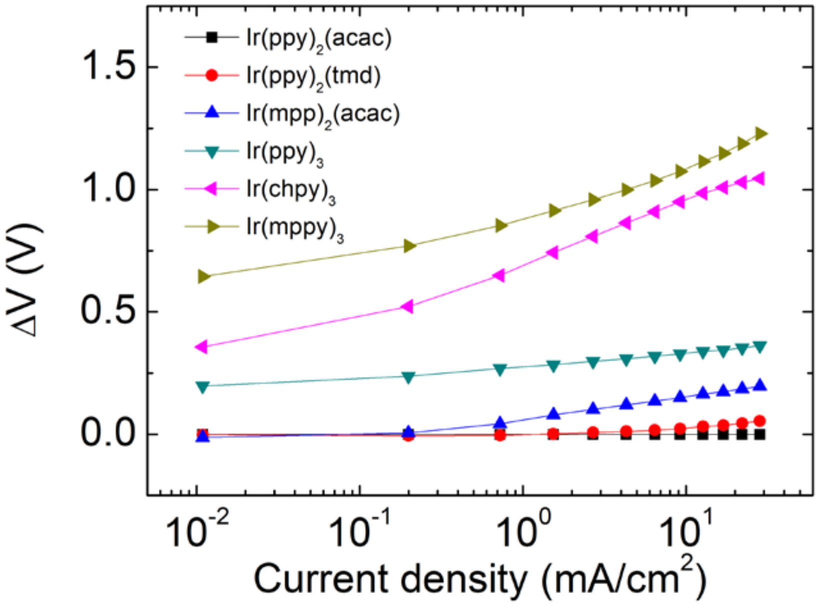

Figure 4.6 Driving voltage difference (ΔV) from the Ir(ppy)$_2$(acac) doped device, against the current density of OLEDs depending on the emitter.

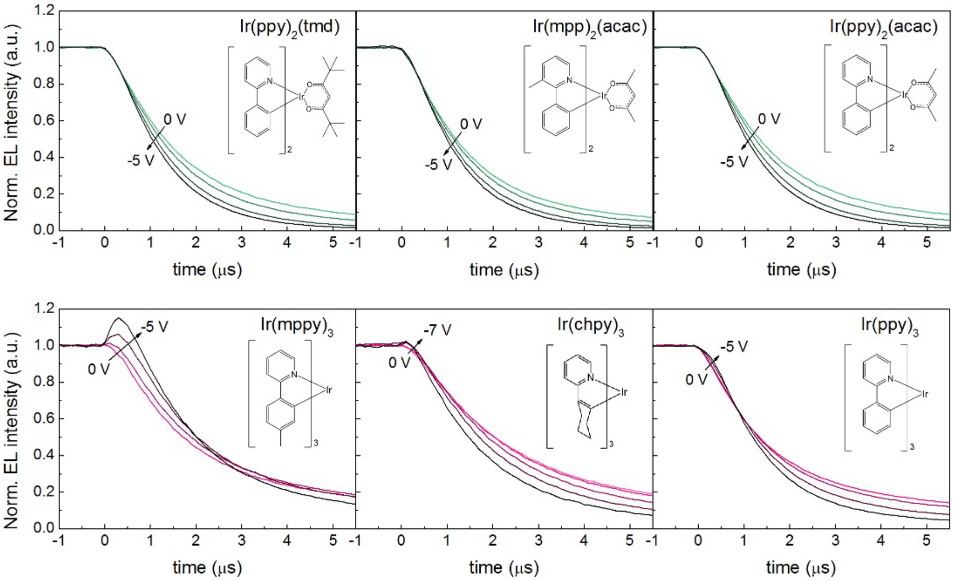

Figure 4.7 Transient electroluminescence characteristics of OLEDs with various Ir dopants. The top three are for heteroleptic dopants and the bottom three are for homoleptic dopants.

on the recombination of residual trapped charges in the dopant, which accelerates the process with increasing reverse bias.[19,69,70] Dopants with higher IP [Ir(mppy)$_3$ and Ir(chpy)$_3$], corresponding to a deeper ΔE_t, resulted in higher overshoots than the device with the lower IP dopant [Ir(ppy)$_3$]. However, the device with the Ir(mpp)$_2$acac having a similar IP with Ir(mppy)$_3$ and Ir(chpy)$_3$ interestingly doesn't exhibit any overshoot. The *J–V–L* characteristics and transient EL measurements indicate that LR is dominant in the devices with the heteroleptic dopants and that TAR is dominant in those with the homoleptic dopants.

Still, however, it is unclear why the heteroleptic and homoleptic Ir(III) complex-doped devices give different charge trapping and recombination mechanisms. It is clear now ΔE_t alone cannot explain the difference of the charge trapping and recombination mechanism as manifested form the comparison between the Ir(mpp)$_2$acac based device and the homoleptic complex based devices. One needs to notice that the ΔE_t of all the dopants are equal to or larger than 0.3 eV. Instead, the difference in the recombination mechanism between the dopants seems to have better correlation to μ_0 (Table 1). It is known that dopant can be considered as a dipole trap and affects charge transport characteristics with energetic disorder arisen from dipole-charge interaction.[44,71-73] This approach successfully explained the field dependent mobility of molecularly doped system with polar dopant by modifying the Bässler’s Gaussian disorder model. Even with the previously reported results on dipole-charge interaction in literature, its effect on the recombination process has not considered much in organic photonic devices to our best knowledge.

4.4 Simulation parameters

Built-in potential is used to be defined as the work function difference between contacts. But in the multilayer stacked devices, interface dipole can shift vacuum level, hence changing the built-in potential of devices. In experimental data, cut-in voltages in the J-V characteristics are different for devices. So built-in potential is a fitting parameter in this modeling. Instead of using arbitrary value to fit the J-V, we used values obtained from Capacitance-Voltage measurement. We defined the built-in potential as the intersection between the baseline and tangent at the point where capacitance increases (Figure 4.8). Since there is an abrupt increase in charge density with the contribution of drift current immediately after the built-in potential to form a flat band condition, from the definition of capacitance($C = \frac{\partial Q}{\partial V}$), This is not a strict value, but it is reasonable.

Measured time-of-flight (TOF) field dependent mobilities (Figure 4.9), summarized in Table 4.2, were used in the calculation. The blend layer has lower mobility than a single layer because of reduced charge-hopping sites.[74,75] Other parameters not mentioned in the text are summarized in Table 4.3.

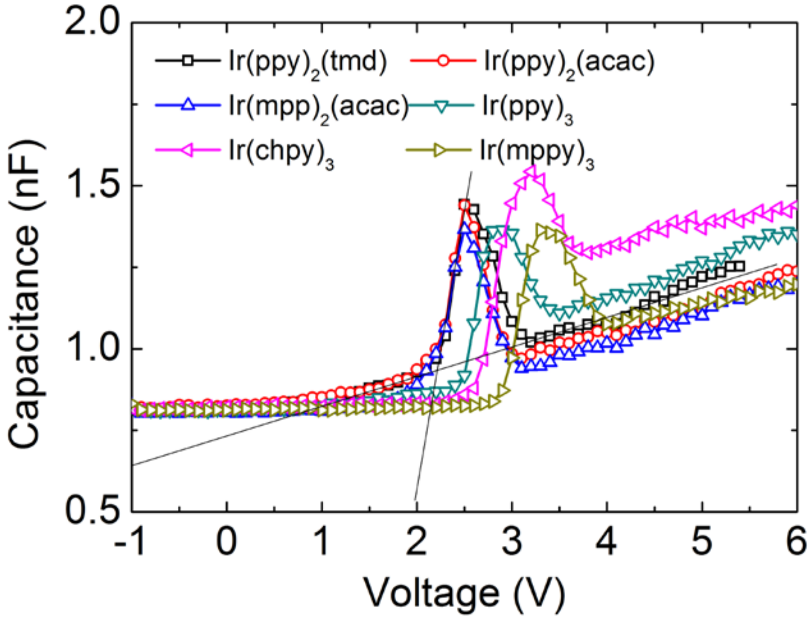

Figure 4.8 Capacitance-voltage plot of devices depending on Ir complex

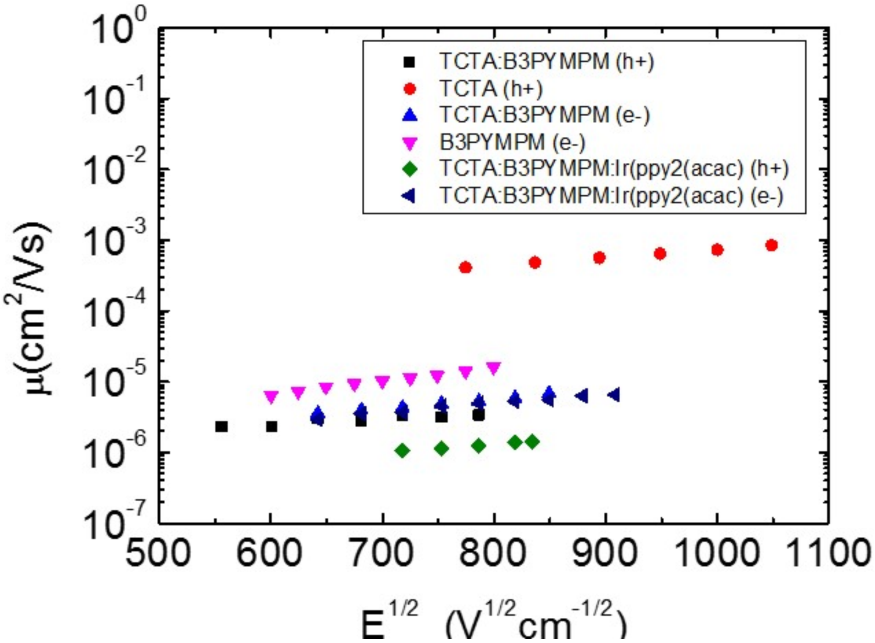

Figure 4.9 Field dependent mobilities measured with time-of-flight equipment

Table 4.2 Time-of-flight measured mobilities and Poole-Frenkel constants of the materials used in the model.

Material	$\mu_{p,0}$ [cm^2/Vs]	γ_p [cm$^{1/2}$/V$^{1/2}$]	$\mu_{n,0}$ [cm^2/Vs]	γ_n [cm$^{1/2}$/V$^{1/2}$]
TCTA	5.0×10^{-5}	2.6×10^{-3}	1.0×10^{-8}	2.0×10^{-3}
B3PYMPM	1.0×10^{-8}	2.0×10^{-3}	4.5×10^{-7}	4.5×10^{-3}
TCTA:B3PYMPM	8.6×10^{-7}	1.8×10^{-3}	5.0×10^{-7}	3.0×10^{-3}

Table 4.3 Simulation parameters used in the drift-diffusion model

Parameter	Symbol	Numerical value
Relative permittivity	ε_r	3.5
Temperature	T	298 K
Discretization distance	Δx	1 nm
Number of Layers	*# of layer*	4
Electron affinity	E_{EA}	1.7/2.1/2.9/2.9 eV
Ionization potential	E_{IP}	5.6/5.8/5.8/6.8 eV
Density of state (EA) (1st, 2nd, 3rd, 4th layer)	N_{EA}	$10^{27}/10^{27}/5\times10^{26}/10^{27}$ m^{-3}
Density of state (IP) (1st, 2nd, 3rd, 4th layer)	N_{IP}	$10^{27}/10^{27}/5\times10^{26}/10^{27}$ m^{-3}
Trap density	N_t	8×10^{25} m^{-3}
Built in potential (In order of Ir(ppy)$_2$(tmd), Ir(ppy)$_2$(tmd), Ir(ppy)$_2$(acac), Ir(mppy)$_3$, Ir(chpy)$_3$, Ir(ppy)$_3$)	V_{bi}	2.15/2.15/2.15 /2.44/2.89/2.60 V
Injection barrier (cathode)	$\phi_{B,e}$	0.3 eV
Injection barrier (anode)	$\phi_{B,h}$	0.3 eV

4.5 Langevin recombination against trap-assisted recombination

Also, charge density, electric field distribution can be calculated with drift-diffusion modeling. Figure 4.10 shows hole, trapped hole and electron density and electric field distribution at $V = V_{bi} + 0.6$. Because built-in potential of the devices are different as in Figure 4.7, we compared distribution using $V\text{-}V_{\underline{bi}}$ as reference. More holes are trapped when doped with homoleptic dopant which have high μ_0 and due to electric field formed by trap (Figure 4.11), density of hole and electron is reduced compared to heteroleptic dye doped devices. As a result, rate of Langevin recombination is higher in heteroleptic dye doped system, whereas rate of trap assisted recombination is higher in homoleptic dye doped system (Figure 4.12).

In order to intuitively see the dominant recombination effect, we calculated P_L depending on the capture radius (or μ_0) and ΔE_t (Figure 4.13). The calculated P_L values of the heteroleptic dopants were 0.72, 0.68, and 0.65 for Ir(ppy)$_2$(tmd), Ir(mpp)$_2$(acac), and Ir(ppy)$_2$(acac), respectively. For the homoleptic dopants, the P_L values were 0.31, 0.26 and 0.25 for Ir(mppy)$_3$, Ir(chpy)$_{3,}$ and Ir(ppy)$_3$, respectively.

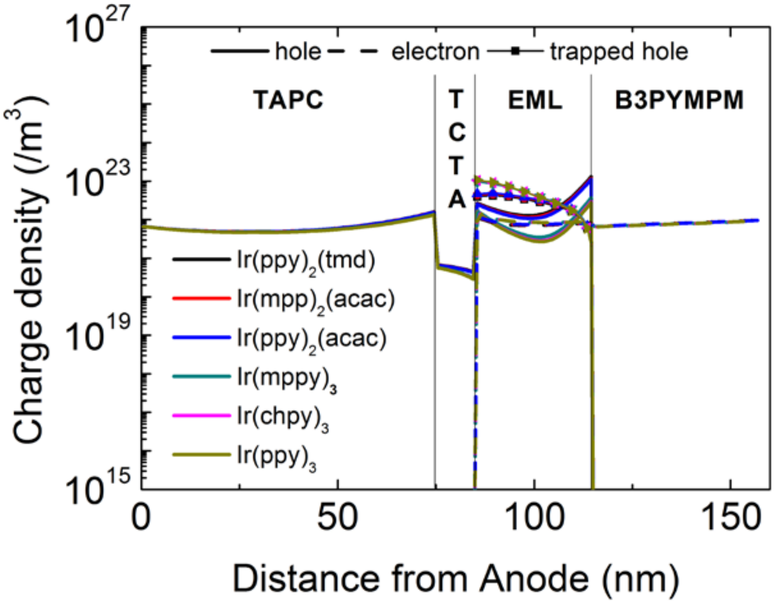

Figure 4.10 Hole, trapped hole and electron distribution in the device depending on phosphorescent emitters.

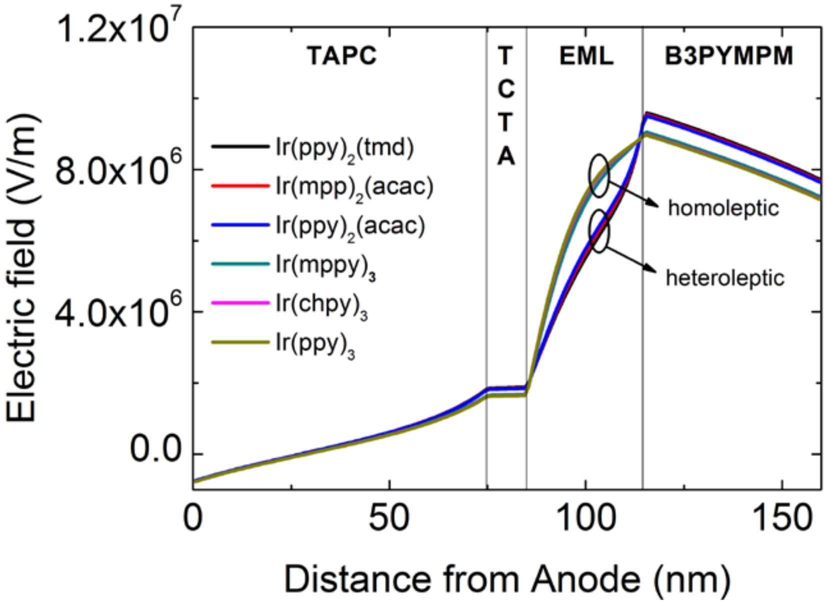

Figure 4.11 The electric field distribution in the devices depending on phosphorescent emitters

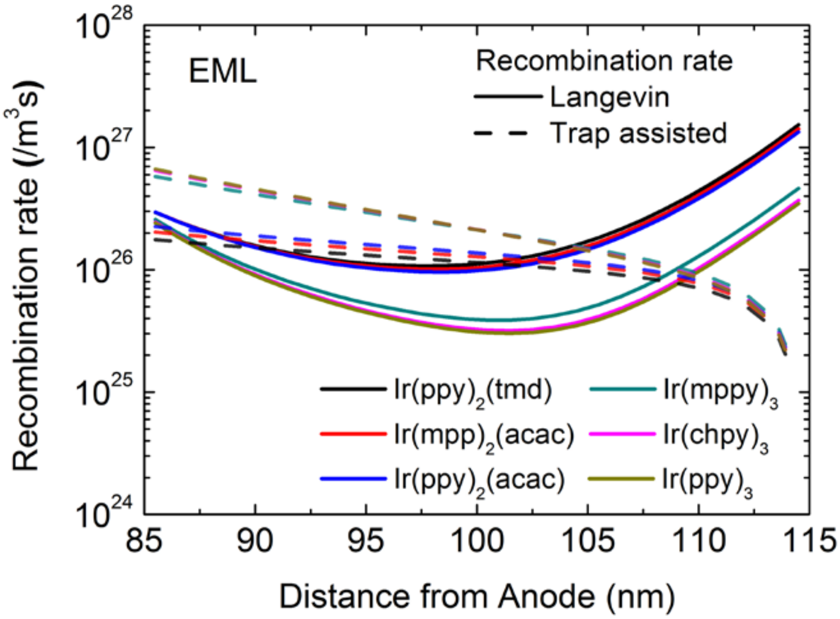

Figure 4.12 Distribution of Langevin and trap assisted recombination rate depending on phosphorescent emitters.

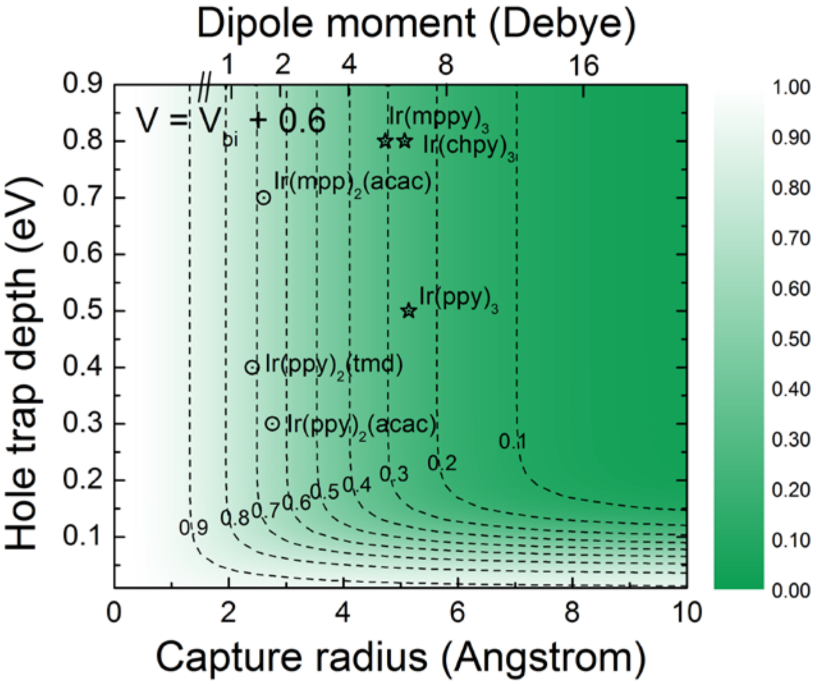

Figure 4.13 Contour plot of simulated portion of Langevin recombination against trap-assisted recombination as functions of capture radius or static dipole moments and ΔE_t of dopants in the device.

The theoretical calculation predicts that LR will be dominant in the heteroleptic complex doped OLEDs and that TAR will dominate in homoleptic complex-doped OLEDs. These results are consistent with the experimental results, showing that the difference in the recombination mechanism is due to different S or μ_0 between the homoleptic and heteroleptic Ir(III) complexes. To generalize the effect of the μ_0 on the recombination mechanism, we calculated P_L as functions of the capture radius and ΔE_t. Figure 4 presents that the effect of ΔE_t becomes saturated when the ΔE_t is > 0.25 eV. This is because the detrapping effect of a hole captured at the dopant decreases markedly with increasing ΔE_t. Above ΔE_t of 0.25 eV, the capture cross radius, therefore μ_0 of the dopant is the major factor that determines P_L. This result indicates that μ_0 of the dopant is a crucial factor in determining the recombination mechanism. Also, the distribution charge (Figure 4.14), electric field (Figure 4.15), and resulting recombination rates (Figure 4.16) are calculated depending on the concentration of Ir(ppy)3. As doping concentration increases, trapping of charges also increases, reducing the concentration of free carriers and reduces P_L.

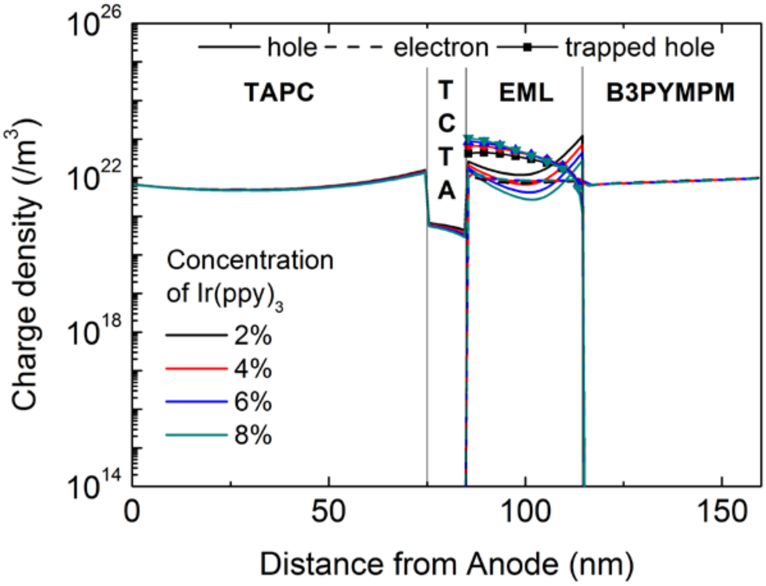

Figure 4.14 Hole, trapped hole and electron distribution in the device depending on the concentration of Ir(ppy)$_3$.

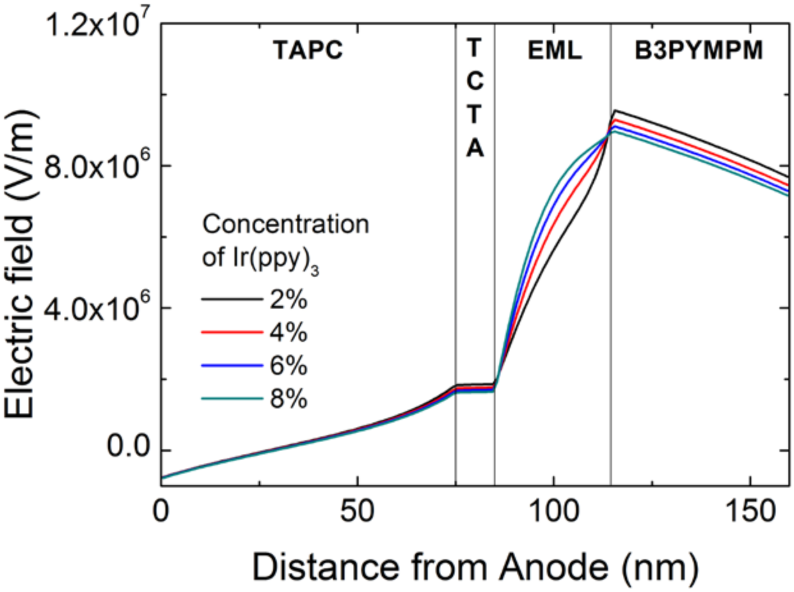

Figure 4.15 The electric field distribution in the devices depending on the concentration of Ir(ppy)$_3$.

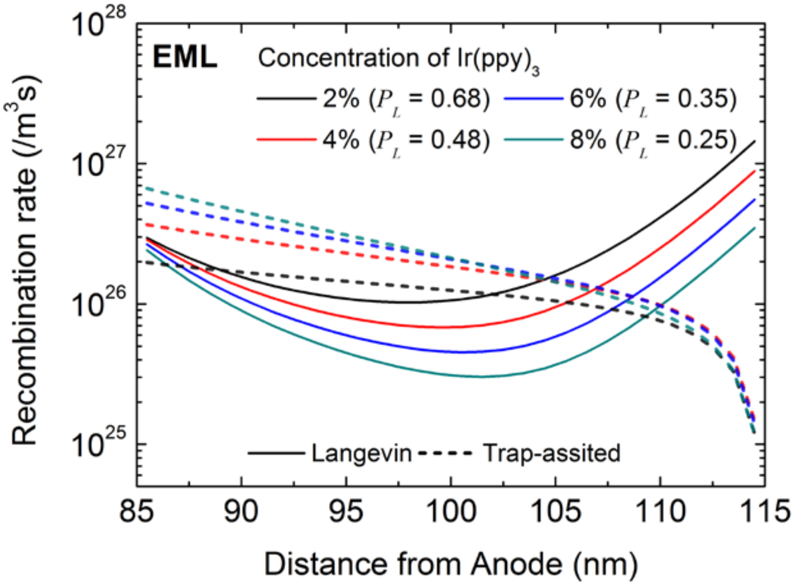

Figure 4.16 Distribution of Langevin and trap assisted recombination rate depending on the concentration of Ir(ppy)$_3$.

4.6 Effect of energetic disorder due to dipoles

In the drift-diffusion mode, differences of energetic disorder due to the dipole moment of the emitter was not addressed. The dipole moment of emitter can be an additional source of energetic disorder, resulting in reduced effective mobility. These effects should also be taken into account in order to know the exact effect of μ_0 on recombination mechanism. Therefore, we analyzed the effect of the μ_0 on carrier mobility using the correlated disorder model (CDM) and the resulting effect on the recombination. First of all, the disorder parameter, σ_d , due to the dipole moment of the dopant was analytically calculated using the expression derived by Young[76],

$$\sigma_d = 0.0707 c^{0.5} \mu_0 / (a^2 \varepsilon) \tag{4-1}$$

where c is the volume concentration, μ_0 is the dipole moment of the dopant, a is the lattice spacing and ε is the relative dielectric constant. Table 4.4 shows the calculated σ_d depending on the dopants we used in our study. We used c = 0.08, a = 1 nm and ε = 3.5 for the calculation.

Contribution of the disorder parameter to total mobility was calculated using the following expression[77]

$$\mu = \mu_c \exp(-2\gamma\rho) \exp\left[-\frac{9}{25}\left(\frac{\sigma}{kT}\right)^2 + C_1 F^{1/2} \left[\left(\frac{\sigma_d}{kT}\right)^{3/2} - \Gamma \right] (e\rho / \sigma_d)^{1/2} \right] \tag{4-2}$$

Table 4.4 Dipole moment of the dopants and resulting σ_d

	Ir(ppy)$_2$(tmd)	Ir(mpp)$_2$(acac)	Ir(ppy)$_2$(acac)
μ_0 (Debye)	1.40	1.64	1.83
σ_d (eV)	0.0080	0.0094	0.0105
	Ir(mppy)$_3$	Ir(chpy)$_3$	Ir(ppy)$_3$
μ_0 (Debye)	5.38	6.18	6.36
σ_d (eV)	0.0307	0.0353	0.0363

where μ_c is a prefactor, γ is the decay radius of a spherical wave function of the electron on the dipolar hopping center, ρ is average distance between dopant molecule (this can be calculated with $\rho = (M / Apc)^{1/3}$), *C1* is constant (0.78) and Γ is positional disorder. To calculate value of equation (4-2), total disorder, σ , the sum of contribution of all disorder the total energetic disorder ($\sigma^2 = \sigma_d^2 + \sigma_p^2 + \sigma_{vdw}^2$) should be considered. The contribution of Van der Waals interaction on the disorder is experimentally determined. Assuming contribution of the other disorder parameter ($\sigma_p^2 + \sigma_{vdw}^2$), the total energetic disorder can be calculated. With this disorder parameter, we calculated approximate value of mobility due to disorder at 10^6 V/m (Figure 4.14), assuming $\mu_c = 1\ cm^2 / Vs$, $2\gamma\alpha = 10$ and $\Gamma = 2$. In 0.05 ~ 0.2 eV range of $\sigma_p^2 + \sigma_{vdw}^2$, mobility difference due to dipole moment of the emitter 2 times or less. To see the effect of mobility on recombination characteristics, we simulated the device depending on the hole and electron mobilities in the emissive layer (Figure 4.15). The hole density near the TCTA/EML interface and the electron density near the EML/B3PYMPM interface increase with decreasing of the mobility because of the mobility gap between transporting layer and the EML. As a result, the portion of Langevin recombination ($P_L = \int R_L dx / \int (R_L + R_{pt}) dx'$) increases with the decrease of the mobility in the EML. This result is consistent with the previous results which reported the charge density dependent recombination mechanism.[12] Comparing the result of μ_0 and $\mu_0 / 2$ (zero mobility of electron and hole reduced to half), the increase in P_L is just 0.03.

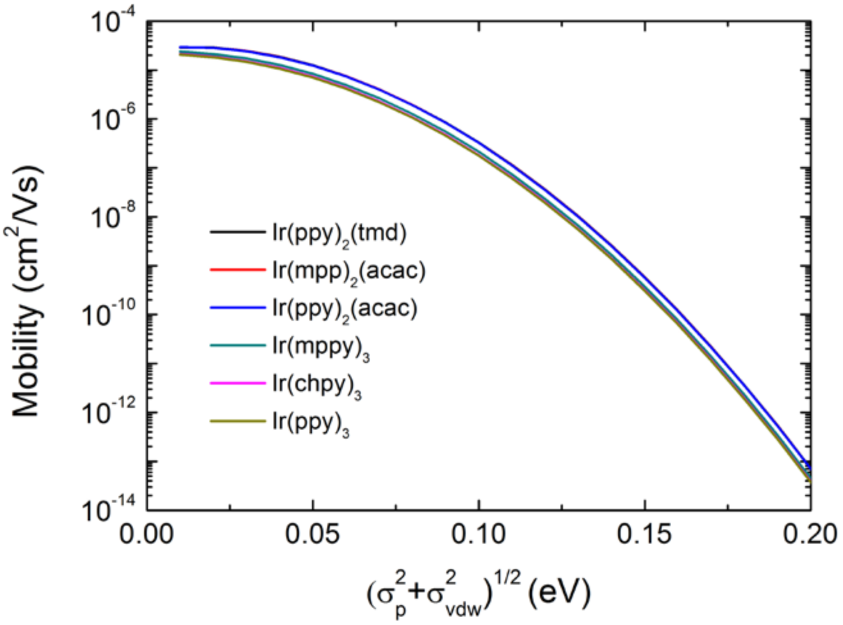

Figure 4.17 Mobility derived from correlated disorder model depending on $\sigma_p^2 + \sigma_{vdw}^2$

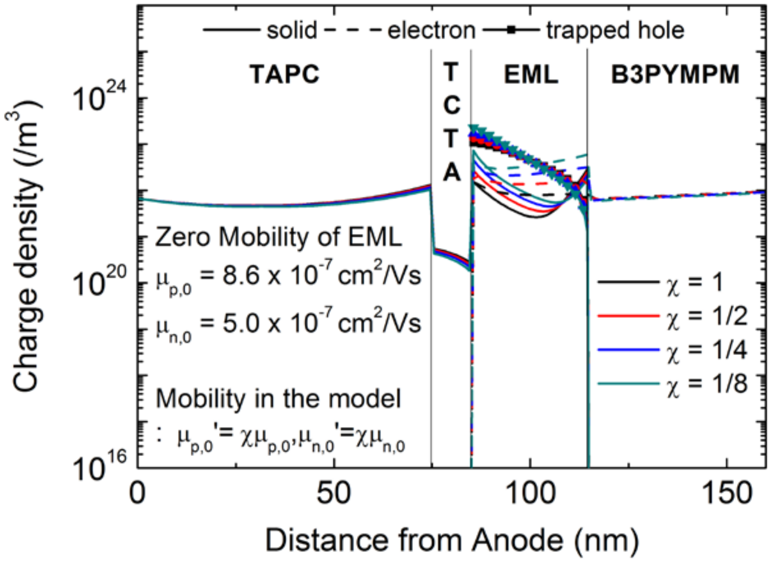

Figure 4.18 Distribution of charge density depending on the hole mobility of EML

.

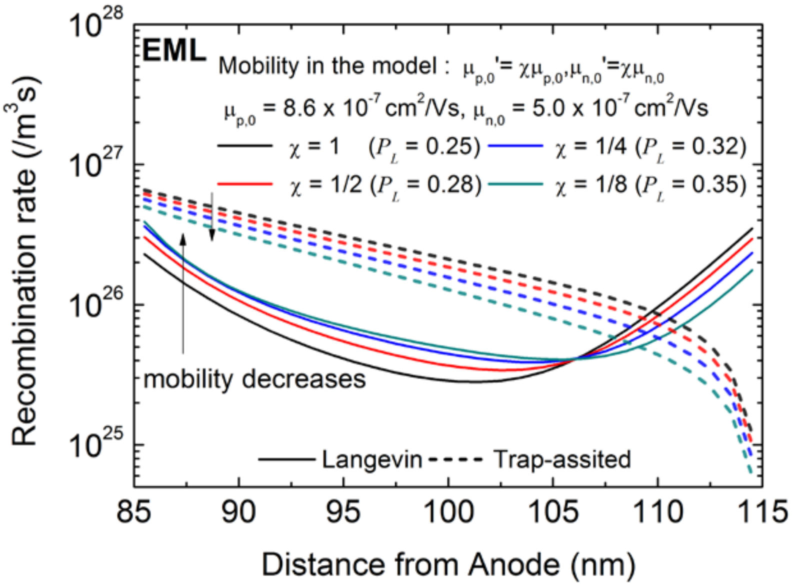

Figure 4.19 Distribution of recombination rate depending on the hole mobility of EML. Corresponding P_L are shown in legend.

4.7 Discussions

The simulation results are based on a number of assumptions that require further discussion.. First, the effects of the μ_0 and ΔE_t of the dopants and carrier density on mobility were not considered in the simulations, and inclusion of these parameters may leads to different results. The time-of-flight (TOF) mobilities of the non-doped emitting layer (TCTA:B3PYMPM mixed host) were used for simulation of the doped systems neglecting the effects of the dopants and carrier density on the mobilities. However, these have only a minimal effect on the calculation results, as discussed below. Among the factors modifying the mobility, increased carrier density will to increase the mobility in disordered systems[78,79], however, this effect is limited in OLEDs because of low carrier densities. The average carrier density in the EML of the devices is ~ 6.0×10^{16} cm^{-3} at a high current density of 20 mA/cm^2 (Figure S1). The increments in the mobility at this carrier density is about 1.5 times that of the TOF mobility assuming an energetic disorder of 0.1 eV.[78] The effect of dopant μ_0 on mobility in the mixed host system has been analyzed using the correlated disorder model based on the dipole glass model[77,80], the effect of the dipole on carrier mobility has also been studied using Monte Carlo simulation[81], with similar results. The mobility change due to μ_0 is negligible for heteroleptic dyes and the mobility decreases by half at most for homoleptic dyes as described in the chapter 4.6. Charge trapping on dopant molecules can also reduce the mobility, and this is indeed the case for shallow dopants. However, it has been reported that the mobility does not change much by doping emitting dyes in disordered emitting layers if $\Delta E_t \geq 0.3$ eV.[82,83] The addition of these effects (μ_0, ΔE_t and carrier density) from the doping of Ir-complexes in our system is expected to reduce the mobility by less than half of the magnitude of the TOF mobility (low carrier density) of the non-doped host at most. The effect of the reduced mobility on P_L was simulated using the drift-diffusion model and P_L was found to increase slightly (~0.03) if the hole and electron mobility in the EML was reduced by half, indicating that the results described in the previous section are valid even when the effects of μ_0, ΔE_t and carrier density on charge mobility are included in the simulation.

Second, we used ΔE_t values based on the energy levels of the host and the dopants obtained from CV measurements. The IP of dopant molecules in films will differ from values measured in solutions due to the polarization effect. Unfortunately, it is very difficult to determine the energy levels of the dopants accurately in films, and most previous studies used the ΔE_t values defined in this study. Therefore, the definition of ΔE_t used in this study is consistent with the literature. This does not necessarily mean than the values used in this study are the real trap depths in the material systems; The influence of dopant μ_0 on ΔE_t requires further study. It is unlikely, however, that the polarization effect will change the absolute values by more than 0.2 eV given the small dielectric constants of organic semiconductors. For instance, the ΔE_t of Ir(ppy)$_3$ in TCTA is 0.5 eV in this study compared to 0.4 eV measured by UPS.[84] If this is the case, the simulation results related to μ_0 obtained in this study are still very much valid because the effect of ΔE_t becomes negligible at ΔE_t > 0.25 eV.

Third, we did not consider the effects of aggregation of dopant molecules and charge transport through aggregate networks.[85] These effects become more significant as the concentration and dopant μ_0 increase and the size of dopants decreases.[86] These effects may explain the differences in transient EL decay patterns and overpotentials among the homoleptic dyes. Ir(chpy)$_3$ and Ir(ppy)$_3$ have larger μ_0 values and smaller sizes than Ir(mppy)$_3$ and hence a greater tendency to aggregate, promoting charge transport through the aggregates, less accumulated charge on the dopant molecules, less pronounced initial delay or overshoot in the transient EL decay curves, and a lower driving voltage. Dopant aggregation explains the experimental observations from the transient EL decay patterns of the different homoleptic dyes. Based on this discussion, we can state with certainty that the simulation results are valid for our system.

The TAR process in OLEDs generally leads to many more accumulated charge carriers on the dopants, where the IP or EA of the dopants are within the bandgap of the host layer[18,49-55], whereas LR attributes to fewer trapped charge carriers in OLEDs under an external bias. The accumulated polarons in the dopant state of the OLEDs potentially hinder the effective mobility of the injected charge carriers and annihilates the generated excitons as well as inducing an unnecessary local-field in the OLEDs during operation. Therefore, LR is preferable to TAR for high-performance OLEDs.[19] In contrast, spin mixing and the resulting conversion of triplet to singlet excitons in recently studied phosphorescent or thermally assisted delayed fluorescent (TADF) dye-sensitized fluorescent OLEDs favor TAR on the sensitizers over LR on host molecules[87] since triplet harvesting OLEDs utilizing either phosphorescent or TADF dyes have a large energy gap between host materials. Although we used phosphorescent OLEDs in this study, these findings can be applied generally to fluorescent and TADF OLEDs where the molecules can be designed to have large (donor-acceptor structure) or small (donor-acceptor-donor structure) μ_0 values. Conversely, recombination between dissociated electrons and holes in photovoltaics operates as a loss channel and should be avoided.

4.6 Conclusion

We showed, through experiments and the analysis using the drift-diffusion model which considers the S of the dopant based on dipole trap theory, that the μ_0 of the dopant is a major factor dictating the recombination mechanism in dye-doped OLEDs if the ΔE_t is larger than 0.25 eV where the detrapping effect diminishes. LR becomes dominant over TAR as the μ_0 of the dye decreases. This can be readily understood because dopants with larger μ_0 have larger S and thus easily capture charges passing by. As the traps become shallower than 0.1 eV, LR becomes dominant over TAR regardless of how large the μ_0 of the dyes is, due to the detrapping effect.

Although we used phosphorescent OLEDs doped with homoleptic (large μ_0) and heteroleptic (small μ_0) Ir(III) complexes, these findings can be applied generally to fluorescent and TADF OLEDs and will be useful for phosphorescent and TADF sensitized fluorescent OLEDs where recombination sites play important roles. Drift-diffusion modeling combined with dipole trap theory can be a useful tool for obtaining insights and designing efficient OLEDs.

Appendix : MATLAB code of drift-diffusion model

Fix_VAR.mat is a collection of variables used in the calculation. The following values must be defined before the calculation.

ELECVOLT = 1.6022e-19;

EPSFREE = 8.8542e-12;

HBAR = 1.0546e-34;

KB = 1.3807e-23;

PI = 3.1416;

MELEC = 9.1095e-31;

STEPSIZE = 1e-9;

The following MATLAB code is used to calculate the distribution of charges, electric fields, and recombination rates of Ir(ppy)$_2$(tmd) doped device at $V = V_{bi} + 0.6$. This code consists of several m-files, so each one must be saved separately (Main_Calc.m, ConTrap_DD.m, Continuity_DD.m, …) for proper operation. Input of the device parameters and execution of program are carried out with Main_Calc.m. Also, the '...' operator is used when the code is long and needs to be passed down to the next line. Whether these operators are left or deleted, the code will work fine.

```
% The following code should be saved as Main_Calc.m


clear

Start_Time = datetime

format long e


global STEPSIZE KB ELECVOLT EPSFREE HBAR PI MELEC

load Fix_VAR



options = odeset('RelTol', 1e-4,'NonNegative',(1:220));



global Steps ;

global Temp;

global Total_thick;

global StepsA StepsB StepsC Eps

global Index_Interface Num_Layers EA_Barrier IP_Barrier global

Layer_Start Layer_End

global N0 dop Eactp Eactn TrapOn_e TrapOn_h

global Dopant_Layer Nc Nv Cap_Area

global Layer_thick EA_lv IP_lv Layer_material EPSREL

global TIMESTEP Vbi Phi_B_e Phi_C_e Phi_B_h Phi_C_h

global Mu_p0 Mu_n0 Gamma_n Gamma_p tol Vapp Recomb R_C

global p_Trap_Recomb n_Trap_Recomb

global FD n_Trap_as p_Trap_as
```

```
%%%%%%%%%%%%%%%%%%%%%%%%%%%%%%%%%%%%%%%%%%%%%%%%%%%%%%%%%%%%%%%%%%%%%%%%%%%

Layer_thick    = [75 10 30 45];
EA_lv          = [1.7 2.1 2.9 2.9];
IP_lv          = [5.6 5.8 5.8 6.8];

EPSREL         = 3.5      ;

Temp           = 298   ;
Nc             = [1e27 1e27 5e26 1e27];
Nv             = [1e27 1e27 5e26 1e27];
N0             = 1e27;

R_C = ELECVOLT^2/(4*PI*EPSREL*EPSFREE*KB*Temp);

Phi_B_e        = 0.3;
Phi_C_e        = 3-Phi_B_e;
Phi_B_h        = 0.3;
Phi_C_h        = 3-Phi_B_h;

Mu_n0          = [1e-8 1e-12 5e-11 4.5e-11];
Gamma_n = [2e-4 2e-4 3e-4 4.5e-4];
Mu_p0          = [6.3e-7 5e-9 8.6e-11 1e-10];
Gamma_p = [6.7e-5 2.6e-4 1.8e-4 2e-4];
```

```
FD = 1; %Field dependence in O-O junction

Vbi            = 2.15;

% Ir(ppy)2tmd   Ir(ppy)2acac   Ir(mpp)2acac
% 0.241        0.276         0.261
% 0.4          0.3           0.7
% Ir(ppy)3     Ir(chpy)3      Ir(mppy)3
% 0.514        0.506         0.473
% 0.5          0.8           0.8

TrapOn_e       = 0;
TrapOn_h       = 1;
Dopant_Layer   = 3;
Dop            = 8e-2;
Radius         = [0.241]*1e-9;

Eactn          = 0.3;
Eactp          = 0.4;
Tol            = 0.005;
information = 'dipole_V_Vbi_0.6_Ir(ppy)2tmd';
%%%%%%%%%%%%%%%%%%%%%%%%%%%%%%%%%%%%%%%%%%%%%%%%%%%%%%%%%%%%%

Time_Total  = 0.5;
Time_Steps  = 1001;
Tin        = 0:Time_Total/(Time_Steps-1):Time_Total;
```

```
Tin        = Tin';

TIMESTEP       = Time_Total/(Time_Steps-1);

Total_thick = sum(Layer_thick);
Num_Layers  = length(Layer_thick);
Mu_n       = ones(1, Total_thick);
Mu_p       = ones(1, Total_thick);

x  = 1 : Total_thick;
x  = x-STEPSIZE*1e9/2;
x_ = 1 : Total_thick-1;
x_V= [0 x Total_thick];

for m = 1 : Num_Layers-1
   Index_Interface(m) = sum(Layer_thick(1:m));
   EA_Barrier(m) = EA_lv(m+1)-EA_lv(m);
   IP_Barrier(m) = IP_lv(m+1)-IP_lv(m);
end

for m = 1 : Num_Layers
   if m==1
      Layer_Start(m)  = 1;
   else
      Layer_Start(m)=Index_Interface(m-1)+1;
   end
```

```
   Layer_End(m) = Layer_Start(m)+Layer_thick(m)-1;
end

for m =1 : Num_Layers
   Mu_n(Layer_Start(m):Layer_End(m)) = ...
Mu_n(Layer_Start(m):Layer_End(m)) * Mu_n0(m);
   Mu_p(Layer_Start(m):Layer_End(m)) = ...
Mu_p(Layer_Start(m):Layer_End(m)) * Mu_p0(m);
end

Eps        = EPSREL * EPSFREE;
Steps      = Total_thick +1;

p_Free0 = 1e19*zeros(1, Total_thick);
n_Free0 = 1e19*zeros(1, Total_thick);
p_Trap0 = 1e19*zeros(1, Total_thick);
n_Trap0 = 1e19*zeros(1, Total_thick);

StepsA = 1: Steps-1;
StepsB = 2: Steps-2;
StepsC = 1: Steps-2;

data_p_Free(:,1)  = x';
data_n_Free(:,1)  = x';
data_p_Trap(:,1)  = x';
data_n_Trap(:,1)  = x';
```

```
data_F(:,1)      = x';

data_V(:,1)      = x_V';

data_V_cat(:,1)   = x';

data_R_rate(:,1)= x';


x_eml = ((0:29)+0.5);

data_R_t_rate(:,1)= x_eml';

data_J_dis(:,1) = x_';

data_J_dev(:,1) = x_';

data_J_sum(:,1) = x_';


Vapp        = 0;

y0         = [p_Free0 n_Free0];

[Tout yMat]  = ode15s('Continuity_DD', Tin,y0,options);

yini        = yMat(end,:);


V    = Vbi + 0.6;

Vl = length(V);


n_Free      = zeros(Time_Steps, Total_thick);

p_Free      = zeros(Time_Steps, Total_thick);

n_Trap      = zeros(Time_Steps, Total_thick);

p_Trap      = zeros(Time_Steps, Total_thick);

Mu_p        = zeros(Time_Steps, Total_thick);

Mu_n        = zeros(Time_Steps, Total_thick);

yMat        = zeros(Time_Steps, 4*Total_thick);
```

```
for j= 1 : Vl
   x0 = clock;
   tic
   y00     = [yini p_Trap0 n_Trap0];

   Vapp   = V(j);
   Cap_Area      = radius^2*pi;

   [Tout yMat]  = ode15s('ConTrap_DD', Tin,y00,options);

   TimeEvol_on;

   J_device    = Jn + Jp;
   J_disp     = Eps*(F(Time_Steps,:)-F(Time_Steps-...
1,:))/TIMESTEP;
   J_dispM    = (J_disp(StepsC)+J_disp(StepsC+1))/2;
   J_sum      = J_device + J_dispM;

   data_J_dis(:,j+1)   = J_dispM';

   V_device(1) = 0;
   J_val = median(J_sum);

   for i = 1 : Steps
      if i==1
```

```
          V_device(i+1) = V_device(i) - F_if(i) ...
*(STEPSIZE/2);
       elseif i==Steps
          V_device(i+1) = V_device(i) - F_if(i) ...
*(STEPSIZE/2);
       else
          V_device(i+1) = V_device(i) - F_if(i) *(STEPSIZE);
       end
   end

   data_p_Free(:,j+1)  = p_Free(Time_Steps,:)';
   data_p_Trap(:,j+1)  = p_Trap(Time_Steps,:)';
   data_n_Free(:,j+1)  = n_Free(Time_Steps,:)';
   data_n_Trap(:,j+1)  = n_Trap(Time_Steps,:)';
   data_F(:,j+1)      = F(Time_Steps,:)';
   data_F_if(:,j+1)    = F_if';
   data_V(:,j+1)      = V_device';
   data_R_rate(:,j+1)  = Recomb';

   data_J_dev(:,j+1)   = J_device';
   data_J_sum(:,j+1)   = J_sum';
   data_EA_band(:,j+1)= -data_V(:,j+1)-EA_lv(1);
   data_IP_band(:,j+1)= -data_V(:,j+1)-IP_lv(1);
   data_R_t_rate(:,j+1) = p_Trap_Recomb';
   data_p_Trap_as(:,j+1)  = p_Trap_as';
   data_n_Trap_as(:,j+1)  = n_Trap_as';
```

```
R_L=trapz(Recomb(Layer_Start(Dopant_Layer):Layer_End(Dopant_Laye
r)));
    R_t=trapz(p_Trap_Recomb);
    R_ratio = R_L/(R_L+R_t);
    data_R_ratio(j,:) = [Vapp R_ratio];

    for i = 1 : Num_Layers-1
        data_EA_band(Layer_Start(i+1)+1:end,j+1) =  ...
data_EA_band(Layer_Start(i+1)+1:end,j+1) - EA_Barrier(i);
        data_IP_band(Layer_Start(i+1)+1:end,j+1) =  ...
data_IP_band(Layer_Start(i+1)+1:end,j+1) - IP_Barrier(i);
    end

    data_JV(j,:)        = [Vapp J_val etime(clock,x0)];

    y00 = yMat(end,:);

    toc
end

Fin = [F_if(1) F_if(end)];

timenow=datestr(now,'yymmdd');
filename = sprintf('%s_%s.mat',timenow,information);
```

```
temp_ratio  = data_J_dis(:,2:end)./data_J_sum(:,2:end);
plot(x_,J_device,x_,J_dispM,x_,J_sum)

data_current = [x_', J_device', J_dispM', J_sum'];

[Jn0 JnL Jp0 JpL]...
=BOUNDARY_CONDITION(Mu_n(end,:),Mu_p(end,:),Eps, ...
n_Free(end,:), p_Free(end,:), Fin,  Phi_B_e, Phi_C_e, ...
Phi_B_h, Phi_C_h);
JnF=[Jn0 Jn JnL]';
data_Jratio = [x_' temp_ratio];

JhF=[Jp0 Jp JpL]';
JsumF=JnF+JhF;

End_Time = datetime;
Total_Time_Ellapsed = End_Time-Start_Time;beep;
save(filename);

% The following code should be saved as Continuity_DD.m

function dy = Continuity_DD(t, y)

global STEPSIZE KB ELECVOLT EPSFREE HBAR PI MELEC
global Steps;
global Temp;
```

```
global Total_thick;
global StepsA StepsB StepsC Eps
global Index_Interface Num_Layers EA_Barrier IP_Barrier
global Layer_Start Layer_End int
global  EPSREL TIMESTEP Vbi Phi_B_e Phi_C_e Phi_B_h Phi_C_h
global Mu_n0 Mu_p0 Gamma_n Gamma_p tol Vapp Recomb
global R_C FD Nc Nv



y=y';

for i= 1: Num_Layers
p_Free(Layer_Start(i):Layer_End(i))     = ...
y(Layer_Start(i):Layer_End(i));
n_Free(Layer_Start(i):Layer_End(i))     = ...
y(Total_thick+Layer_Start(i):Total_thick+Layer_End(i));
end

F   = zeros(1, Total_thick);

Rho   = (p_Free - n_Free) * ELECVOLT ;
[F_latter, F, F_if] = ...
Fif_SOLVE(Rho, Steps, EPSREL, Vbi, Vapp) ;

Mu_n      = ones(1, Total_thick);
Mu_p      = ones(1, Total_thick);

for m =1 : Num_Layers
   Mu_n(Layer_Start(m):Layer_End(m)) = ...
Mu_n(Layer_Start(m):Layer_End(m)) * Mu_n0(m) ;
```

```
    Mu_p(Layer_Start(m):Layer_End(m)) = ...
Mu_p(Layer_Start(m):Layer_End(m)) * Mu_p0(m) ;
end

[p_drift_forward, p_drift_reverse, n_drift_forward, ...
 n_drift_reverse]   =  Drift(Mu_n, Mu_p, F, n_Free, p_Free);
[p_diff_forward,  p_diff_reverse,  n_diff_forward, ...
n_diff_reverse ]   =  Diff(Mu_n, Mu_p, F, n_Free, p_Free);

Fin = [F_if(1) F_if(end)];
[Jn0, JnL, Jp0, JpL] = ...
BOUNDARY_CONDITION (Mu_n,Mu_p,Eps, n_Free, p_Free, ...
F,  Phi_B_e, Phi_C_e, Phi_B_h, Phi_C_h);

Flux_n_0 = -Jn0/ELECVOLT/STEPSIZE;Flux_n_L = ...
JnL/ELECVOLT/STEPSIZE;
Flux_p_0 = Jp0/ELECVOLT/STEPSIZE;Flux_p_L = ...
-JpL/ELECVOLT/STEPSIZE;

n_forward(StepsA) = n_drift_forward(StepsA) + ...
n_diff_forward(StepsA);
n_reverse(StepsA) = n_drift_reverse(StepsA) + ...
n_diff_reverse(StepsA);

p_forward(StepsA) = p_drift_forward(StepsA) + ...
p_diff_forward(StepsA);
p_reverse(StepsA) = p_drift_reverse(StepsA) + ...
p_diff_reverse(StepsA);

for k= 1:Num_Layers-1
```

```
   Fif(k)      = (F(Layer_End(k))+F(Layer_Start(k+1)))/2;
   f          = 0;

   EA_BarF(k) = abs(EA_Barrier(k));
   IP_BarF(k) = abs(IP_Barrier(k));

   % electron
   if EA_Barrier > 0
       n_reverse(Index_Interface(k)+1) = ...
n_reverse(Index_Interface(k)+1)   * ...
exp(-EA_BarF(k)*ELECVOLT/KB/Temp)*exp(sqrt(f)) ;
   else
       n_forward(Index_Interface(k))   = ...
n_forward(Index_Interface(k))    * ...
exp(-EA_BarF(k)*ELECVOLT/KB/Temp)*exp(sqrt(f));
   end

   % hole
   if IP_Barrier > 0
       p_forward(Index_Interface(k))   = ...
p_forward(Index_Interface(k))    * ...
exp(-IP_BarF(k)*ELECVOLT/KB/Temp)*exp(sqrt(f));
   else
       p_reverse(Index_Interface(k)+1) = ...
p_reverse(Index_Interface(k)+1)   * ...
exp(-IP_BarF(k)*ELECVOLT/KB/Temp)*exp(sqrt(f));
   end

end
```

```
Delta_N(StepsB) = -n_forward(StepsB)-n_reverse(StepsB)...
               +n_forward(StepsB-1)+n_reverse(StepsB+1);
Delta_P(StepsB) = -p_forward(StepsB)-p_reverse(StepsB)...
               +p_forward(StepsB-1)+p_reverse(StepsB+1);

Delta_N(1)     = -n_forward(1)+n_reverse(1+1)...
               +Flux_n_0;
Delta_P(1)     = -p_forward(1)+p_reverse(1+1)...
               +Flux_p_0;

Delta_N(Steps-1)= -n_reverse(Steps-1)+n_forward(Steps-2)...
               +Flux_n_L;
Delta_P(Steps-1)= -p_reverse(Steps-1)+p_forward(Steps-2)...
               +Flux_p_L;

Gamma   = ELECVOLT * (Mu_n + Mu_p)/Eps;
R      = Gamma .* (n_Free .* p_Free );

Delta_P=Delta_P-R;Delta_N=Delta_N-R;

Recomb = R;

dy = [Delta_P Delta_N];
dy = dy';

end

% The following code should be saved as ConTrap_DD.m
```

```
function dy = ConTrap_DD(t, y)

global STEPSIZE KB ELECVOLT EPSFREE HBAR PI MELEC
global Steps;
global Temp;
global Total_thick;
global StepsA StepsB StepsC Eps Rindex
global Index_Interface Num_Layers EA_Barrier IP_Barrier
global Layer_Start Layer_End
global Layer_thick EA_lv IP_lv Layer_material EPSREL
global TIMESTEP Vbi Phi_B_e Phi_C_e Phi_B_h Phi_C_h
global Mu_n0 Mu_p0 Gamma_n Gamma_p tol Vapp Recomb
global p_Trap_Recomb n_Trap_Recomb R_C
global FD FNTN
global N0 dop Eactp Eactn TrapOn_e TrapOn_h N_A N_D  Nc Nv
global Dopant_Layer Cap_Area
global Et sigma_t Nt E_EA E_IP N_C N_V Defect_Trap_On global
n_Trap_Gauss E_Fermi_n n_Trap_as p_Trap_as

y=y';

for i= 1: Num_Layers
p_Free(Layer_Start(i):Layer_End(i))
=y(               Layer_Start(i) :                Layer_End(i));
n_Free(Layer_Start(i):Layer_End(i))     =...
y(Total_thick + Layer_Start(i):Total_thick + Layer_End(i));
p_Trap(Layer_Start(i):Layer_End(i))     =...
y(2 * Total_thick + Layer_Start(i) : 2*  Total_thick +...
Layer_End(i));
n_Trap(Layer_Start(i):Layer_End(i))     =...
```

```
y(3 * Total_thick + Layer_Start(i) : 3*  Total_thick +...
Layer_End(i));
end

F   = zeros(1, Total_thick);

Rho    = (p_Free + p_Trap - n_Free - n_Trap) * ELECVOLT ;
[F_latter, F, F_if] = ...
Fif_SOLVE(Rho, Steps, EPSREL, Vbi, Vapp) ;

Mu_n       = ones(1, Total_thick);
Mu_p       = ones(1, Total_thick);

for m =1 : Num_Layers
   Mu_n(Layer_Start(m):Layer_End(m)) = ...
Mu_n(Layer_Start(m):Layer_End(m)) * Mu_n0(m) .* ...
exp (Gamma_n(m)*sqrt(abs(F(Layer_Start(m):Layer_End(m)))));
   Mu_p(Layer_Start(m):Layer_End(m)) = ...
Mu_p(Layer_Start(m):Layer_End(m)) * Mu_p0(m) .* ...
exp (Gamma_p(m)*sqrt(abs(F(Layer_Start(m):Layer_End(m)))));
end

[p_drift_forward, p_drift_reverse, n_drift_forward, ...
n_drift_reverse]    =  Drift(Mu_n, Mu_p, F, n_Free, p_Free);
[p_diff_forward,  p_diff_reverse,  n_diff_forward, ...
n_diff_reverse ]    =  Diff(Mu_n, Mu_p, F, n_Free, p_Free);

Fin = [F_if(1) F_if(end)];
[Jn0, JnL, Jp0, JpL]=BOUNDARY_CONDITION...
(Mu_n,Mu_p,Eps, n_Free, p_Free, Fin,  Phi_B_e, ...
```

```
Phi_C_e, Phi_B_h, Phi_C_h);
Flux_n_0 = -Jn0/ELECVOLT/STEPSIZE;Flux_n_L = ...
JnL/ELECVOLT/STEPSIZE;
Flux_p_0 = Jp0/ELECVOLT/STEPSIZE;Flux_p_L = ...
-JpL/ELECVOLT/STEPSIZE;

n_forward(StepsA) = n_drift_forward(StepsA) + ...
n_diff_forward(StepsA);
n_reverse(StepsA) = n_drift_reverse(StepsA) + ...
n_diff_reverse(StepsA);

p_forward(StepsA) = p_drift_forward(StepsA) + ...
p_diff_forward(StepsA);
p_reverse(StepsA) = p_drift_reverse(StepsA) + ...
p_diff_reverse(StepsA);

for k= 1:Num_Layers-1

   Fif(k)      = F_if(Layer_End(k)+1);

   if FD == 1
        f          = ELECVOLT*Fif(k)*STEPSIZE/Temp/KB;
   else
        f          = 0;
   end

   EA_BarF(k) = abs(EA_Barrier(k));
   IP_BarF(k) = abs(IP_Barrier(k));

% electron
```

```
   if EA_Barrier > 0
       n_reverse(Index_Interface(k)+1) = ...
n_reverse(Index_Interface(k)+1)   * ...
exp(-EA_BarF(k)*ELECVOLT/KB/Temp)*exp(sqrt(f)) ;
   else
       n_forward(Index_Interface(k))   = ...
n_forward(Index_Interface(k))    * ...
exp(-EA_BarF(k)*ELECVOLT/KB/Temp)*exp(sqrt(f));
   end

   % hole
   if IP_Barrier > 0
       p_forward(Index_Interface(k))   = ...
p_forward(Index_Interface(k))    * ...
exp(-IP_BarF(k)*ELECVOLT/KB/Temp)*exp(sqrt(f));
   else
       p_reverse(Index_Interface(k)+1) = ...
p_reverse(Index_Interface(k)+1)   * ...
exp(-IP_BarF(k)*ELECVOLT/KB/Temp)*exp(sqrt(f));
   end

end

Delta_N(StepsB) = -n_forward(StepsB)-n_reverse(StepsB)...
               +n_forward(StepsB-1)+n_reverse(StepsB+1);
Delta_P(StepsB) = -p_forward(StepsB)-p_reverse(StepsB)...
               +p_forward(StepsB-1)+p_reverse(StepsB+1);
Delta_N(1)     = -n_forward(1)+n_reverse(1+1)...
               +Flux_n_0;
Delta_P(1)     = -p_forward(1)+p_reverse(1+1)...
```

```
               +Flux_p_0;

Delta_N(Steps-1)= -n_reverse(Steps-1)+n_forward(Steps-2)...
               +Flux_n_L;
Delta_P(Steps-1)= -p_reverse(Steps-1)+p_forward(Steps-2)...
               +Flux_p_L;

Gamma       = ELECVOLT * (Mu_n + Mu_p)/Eps;
R          = Gamma .* (n_Free .* p_Free);

Jp(StepsC)     =  ELECVOLT * (p_forward(StepsC)-
p_reverse(StepsC+1))*STEPSIZE;
Jn(StepsC)     = -ELECVOLT * (n_forward(StepsC)-
n_reverse(StepsC+1))*STEPSIZE;

JpF=[Jp0 Jp JpL]';
JnF=[Jn0 Jn JnL]';

JpM = (JpF(StepsA)+JpF(StepsA+1))/2;
JnM = (JnF(StepsA)+JnF(StepsA+1))/2;
JpM = JpM'; JnM = JnM';

Delta_P = Delta_P-R;
Delta_N = Delta_N-R;

Recomb = R;

for k = 1 : Num_Layers
   if k == Dopant_Layer
```

```
       N_t    = N0 * dop;

       Vpt    = ...
abs(JpM(Layer_Start(k):Layer_End(k)))./...
(p_Free(Layer_Start(k):Layer_End(k))*ELECVOLT);
       Vnt    = ...
abs(JnM(Layer_Start(k):Layer_End(k)))./...
(n_Free(Layer_Start(k):Layer_End(k))*ELECVOLT);

       p_d       = TrapOn_h * ...
N_t*(1+(Nc(Dopant_Layer)./...
p_Free(Layer_Start(k):Layer_End(k))-1)*...
exp(-Eactp/(KB*Temp/ELECVOLT))+ELECVOLT/Eps * ...
Mu_n(Layer_Start(k):Layer_End(k)) .* ...
n_Free(Layer_Start(k):Layer_End(k))./...
(p_Free(Layer_Start(k):Layer_End(k)).*Vpt*Cap_Area)).^(-1);
       n_d       = TrapOn_e * ...
N_t*(1+(Nv(Dopant_Layer)./...
n_Free(Layer_Start(k):Layer_End(k))-1)*...
exp(-Eactn/(KB*Temp/ELECVOLT))+ELECVOLT/Eps *...
Mu_p(Layer_Start(k):Layer_End(k)) .*...
p_Free(Layer_Start(k):Layer_End(k))./...
(n_Free(Layer_Start(k):Layer_End(k)).*Vnt*Cap_Area)).^(-1);

       Delta_p_Trap(Layer_Start(k):Layer_End(k))   = ...
TrapOn_h * Cap_Area * Vpt.*((N_t -...
p_Trap(Layer_Start(k):Layer_End(k))).*...
p_Free(Layer_Start(k):Layer_End(k)) - (Nv(k) - ...
p_Free(Layer_Start(k):Layer_End(k)))*...
exp(Eactp/(KB*Temp/ELECVOLT)).*...
```

```
p_Trap(Layer_Start(k):Layer_End(k)));
       Delta_n_Trap(Layer_Start(k):Layer_End(k))   = ...
TrapOn_e * Cap_Area * Vnt.*((N_t - ...
n_Trap(Layer_Start(k):Layer_End(k))).*...
n_Free(Layer_Start(k):Layer_End(k)) - (Nc(k) - ...
n_Free(Layer_Start(k):Layer_End(k)))*...
exp(-Eactn/(KB*Temp/ELECVOLT)).*...
n_Trap(Layer_Start(k):Layer_End(k)));

       Rec_Trap_p  = ELECVOLT/Eps * ...
Mu_n(Layer_Start(k):Layer_End(k)).* ...
n_Free(Layer_Start(k):Layer_End(k)).* p_d;
       Rec_Trap_n  = ELECVOLT/Eps * ...
Mu_p(Layer_Start(k):Layer_End(k)).* ...
p_Free(Layer_Start(k):Layer_End(k)).* n_d;

       Delta_P(Layer_Start(k):Layer_End(k))       = ...
Delta_P(Layer_Start(k):Layer_End(k)) - ...
Delta_p_Trap(Layer_Start(k):Layer_End(k)) - Rec_Trap_n;
       Delta_N(Layer_Start(k):Layer_End(k))       = ...
Delta_N(Layer_Start(k):Layer_End(k)) - ...
Delta_n_Trap(Layer_Start(k):Layer_End(k)) - Rec_Trap_p;

       Delta_p_Trap(Layer_Start(k):Layer_End(k))  = ...
Delta_p_Trap(Layer_Start(k):Layer_End(k))  - Rec_Trap_p ;
       Delta_n_Trap(Layer_Start(k):Layer_End(k))  = ...
Delta_n_Trap(Layer_Start(k):Layer_End(k))  - Rec_Trap_n ;

   else
       Delta_p_Trap(Layer_Start(k):Layer_End(k)) = 0 * ...
```

```
p_Free(Layer_Start(k):Layer_End(k));
       Delta_n_Trap(Layer_Start(k):Layer_End(k)) = 0 * ...
n_Free(Layer_Start(k):Layer_End(k));
   end
end

n_Trap_as = n_d;
p_Trap_as = p_d;
p_Trap_Recomb = Rec_Trap_p;
n_Trap_Recomb = Rec_Trap_n;

dy = [Delta_P Delta_N Delta_p_Trap Delta_n_Trap];
dy = dy';

end

% The following code should be saved as Diff.m

function [p_diff_forward, p_diff_reverse, n_diff_forward,
n_diff_reverse]=Diff(Mu_n, Mu_p, F, n_Free, p_Free)

global STEPSIZE KB ELECVOLT EPSFREE HBAR PI MELEC;
global Steps;
global Temp;


p_diff_element  =
abs(Mu_p*KB*Temp.*p_Free/(ELECVOLT*STEPSIZE^2));
n_diff_element  =
abs(Mu_n*KB*Temp.*n_Free/(ELECVOLT*STEPSIZE^2));
```

```
p_diff_forward   = p_diff_element;
p_diff_reverse   = p_diff_element;
n_diff_forward   = n_diff_element;
n_diff_reverse   = n_diff_element;

end

% The following code should be saved as Drift.m

function [p_drift_forward, p_drift_reverse, ...
n_drift_forward, n_drift_reverse]=...
Drift(Mu_n, Mu_p, F, n_Free, p_Free)

global STEPSIZE
global Steps;
global Temp;
global Total_thick;

p_drift_element = abs(Mu_p.*F.*p_Free/STEPSIZE);
n_drift_element = abs(Mu_n.*F.*n_Free/STEPSIZE);

p_drift_forward = zeros(1, Total_thick);
p_drift_reverse = zeros(1, Total_thick);
n_drift_forward = zeros(1, Total_thick);
n_drift_reverse = zeros(1, Total_thick);

for i = 1 : Steps-1
   if F(i) > 0
   p_drift_forward(i) = p_drift_element(i);
```

```
   p_drift_reverse(i) = 0;
   n_drift_forward(i) = 0;
   n_drift_reverse(i) = n_drift_element(i);
   else
   p_drift_forward(i) = 0;
   p_drift_reverse(i) = p_drift_element(i);
   n_drift_forward(i) = n_drift_element(i);
   n_drift_reverse(i) = 0;
   end
end

end

% The following code should be saved as Fif_SOLVE.m

function [F_former, F, F_if] = ...
Fif_SOLVE(Rho, Steps, EPSRel, Vbi, Vapp)
   global STEPSIZE KB ELECVOLT EPSFREE HBAR PI MELEC

   F_Former_Interface  = zeros(1,Steps);
   F_Former_Position   = zeros(1,Steps-1);
   Allsum = sum(1:Steps-1);
   Sum_Former  = 0 ;
   Sum_Latter  = 0 ;
   for i = 1 : Steps % Thickness + 1
      F_Former_Interface(i) = ...
STEPSIZE/(2*EPSFREE*EPSRel)*(2*sum(Rho(1:i-1))-Allsum);
   end

   for i = 1 : Steps-1
```

```
       F_Former_Position(i) = ...
(F_Former_Interface(i) +  F_Former_Interface(i+1))/2;
   end

   X = (0:1:Steps-1)*1e-9;
   Trapz_F_Former = trapz(X,F_Former_Interface);

   F_Rho_anode    = (Vapp - Vbi - Trapz_F_Former)/...
((Steps-1)*1e-9);
   F_if          = F_Former_Interface + F_Rho_anode;
   F             = (F_if(1:Steps-1)+F_if(2:Steps))/2;
   F_former       = F_Former_Position + F_Rho_anode;
end

% The following code should be saved as BOUNDARY_CONDITION.m

function [Jn0, JnL, Jp0, JpL]=BOUNDARY_CONDITION...
(Mu_n,Mu_p,Eps, n_Free, p_Free, F, Phi_B_e, Phi_C_e,...
 Phi_B_h, Phi_C_h)

global KB ELECVOLT PI
%global STEPSIZE EPSFREE HBAR MELEC
%Layer_thick, Steps, Temp
global Steps;
global Temp TI;

N0  =  1e27;

% nJL, Injection
Rc  = ELECVOLT^2 / (4*pi*Eps*KB*Temp);
```

```
S0  = 16*pi*Eps*(KB*Temp)^2*Mu_n(Steps-1)/ELECVOLT^2;
S1  = (16*PI*Eps*(KB*Temp/ELECVOLT)^2+...
ELECVOLT*abs(F(2)))*Mu_n(Steps-1);
C   = 16*pi*Eps*(KB*Temp)^2*Mu_n(Steps-1)/ELECVOLT^2*N0;
f   = abs(ELECVOLT*F(2)*Rc/(KB*Temp));
psi = 1/f*(1-sqrt(1+2*sqrt(f))) + 1/sqrt(f);
SE  = S0*(1/psi^2-f)/4;

if F(2) > 0
   JnL = C*exp(-(Phi_B_e*ELECVOLT)/(KB*Temp))*...
exp(sqrt(f))-n_Free(Steps-1)*SE;

else
   JnL = C*exp(-(Phi_B_e*ELECVOLT-...
ELECVOLT*F(2)*Rc/4)/(KB*Temp))-n_Free(Steps-1)*S1;

end

% nJ0, Extraction
Rc  = ELECVOLT^2 / (4*pi*Eps*KB*Temp);
S0  = 16*pi*Eps*(KB*Temp)^2*Mu_n(1)/ELECVOLT^2;
S1  = (16*PI*Eps*(KB*Temp/ELECVOLT)^2+...
ELECVOLT*abs(F(1)))*Mu_n(1);
C   = 16*pi*Eps*(KB*Temp)^2*Mu_n(1)/ELECVOLT^2*N0;
f   = abs(ELECVOLT*F(1)*Rc/(KB*Temp));
psi = 1/f*(1-sqrt(1+2*sqrt(f))) + 1/sqrt(f);
SE  = S0*(1/psi^2-f)/4;

if F(1) < 0
   Jn0 = -C*exp(-(Phi_C_e*ELECVOLT)/(KB*Temp))*...
```

```
exp(sqrt(f))+n_Free(1)*SE;
else
   Jn0 = -C*exp(-(Phi_C_e*ELECVOLT+ELECVOLT*F(1)*Rc/4)/...
(KB*Temp))+n_Free(1)*S1;

end

% pJ0, injection

Rc  = ELECVOLT^2 / (4*pi*Eps*KB*Temp);
S0  = 16*pi*Eps*(KB*Temp)^2*Mu_p(1)/ELECVOLT^2;
S1  = (16*PI*Eps*(KB*Temp/ELECVOLT)^2+...
ELECVOLT*abs(F(1)))*Mu_p(1);
C   = 16*pi*Eps*(KB*Temp)^2*Mu_p(1)/ELECVOLT^2*N0;
f   = abs(ELECVOLT*F(1)*Rc/(KB*Temp));
psi = 1/f*(1-sqrt(1+2*sqrt(f))) + 1/sqrt(f);
SE  = S0*(1/psi^2-f)/4;

if F(1) > 0
   Jp0 = C*exp(-(Phi_B_h*ELECVOLT)/(KB*Temp))*...
exp(sqrt(f))-p_Free(1)*SE;

else
   Jp0 = C*exp(-(Phi_B_h*ELECVOLT-...
ELECVOLT*F(1)*Rc/4)/(KB*Temp))-p_Free(1)*S1;

end

% pJL, Extraction
Rc  = ELECVOLT^2 / (4*pi*Eps*KB*Temp);
```

```
S0  = 16*pi*Eps*(KB*Temp)^2*Mu_p(Steps-1)/ELECVOLT^2;
S1  = (16*PI*Eps*(KB*Temp/ELECVOLT)^2+...
ELECVOLT*abs(F(2)))*Mu_p(Steps-1);
C   = 16*pi*Eps*(KB*Temp)^2*Mu_p(Steps-1)/ELECVOLT^2*N0;
f   = abs(ELECVOLT*F(2)*Rc/(KB*Temp));
psi = 1/f*(1-sqrt(1+2*sqrt(f))) + 1/sqrt(f);
SE  = S0*(1/psi^2-f)/4;

if F(2) < 0
   JpL = -C*exp(-(Phi_C_h*ELECVOLT)/(KB*Temp))*...
exp(sqrt(f))+p_Free(Steps-1)*SE;
else
   JpL = -C*exp(-(Phi_C_h*ELECVOLT+ELECVOLT*F(2)...
*Rc/4)/(KB*Temp))+p_Free(Steps-1)*S1;

end

end

% The following code should be saved as TimeEvol_on.m

for i= 1: Time_Steps
   y = yMat(i,:);

   p_Free(i,:)=y(1             :    Total_thick);
   n_Free(i,:)=y(Total_thick+1   : 2 * Total_thick);
   p_Trap(i,:)=y(2 * Total_thick+1: 3 * Total_thick);
   n_Trap(i,:)=y(3 * Total_thick+1: 4 * Total_thick);
   Rho      = (p_Free(i,:) + p_Trap(i,:) - ...
 n_Free(i,:) - n_Trap(i,:)) * ELECVOLT ;%
```

```
    [F_latter, F(i,:), F_if]    = ...
Fif_SOLVE(Rho, Steps, EPSREL, Vbi, Vapp);

    Mu_ns       = ones(1, Total_thick);
    Mu_ps       = ones(1, Total_thick);

    for m =1 : Num_Layers
        Mu_n(i,Layer_Start(m):Layer_End(m)) = ...
Mu_ns(Layer_Start(m):Layer_End(m)) * Mu_n0(m).* exp ...
(Gamma_n(m)*sqrt(abs(F(i,Layer_Start(m):Layer_End(m)))));
        Mu_p(i,Layer_Start(m):Layer_End(m)) = ...
Mu_ps(Layer_Start(m):Layer_End(m)) * Mu_p0(m).* exp ...
(Gamma_p(m)*sqrt(abs(F(i,Layer_Start(m):Layer_End(m)))));
    end

        [p_drift_forward, p_drift_reverse, ...
n_drift_forward, n_drift_reverse]   =  ...
Drift(Mu_n(i,:), Mu_p(i,:), F(i,:), n_Free(i,:),...
p_Free(i,:));
        [p_diff_forward,  p_diff_reverse, ...
n_diff_forward,  n_diff_reverse ]   =  ...
Diff(Mu_n(i,:), Mu_p(i,:), F(i,:), n_Free(i,:), ...
p_Free(i,:));

        n_forward(StepsA) = n_drift_forward(StepsA) ...
 + n_diff_forward(StepsA);n_reverse(StepsA) = ...
n_drift_reverse(StepsA) + n_diff_reverse(StepsA);
        p_forward(StepsA) = p_drift_forward(StepsA) ...
+ p_diff_forward(StepsA);p_reverse(StepsA) = ...
p_drift_reverse(StepsA) + p_diff_reverse(StepsA);
```

```
      for k= 1:Num_Layers-1

          Fif(k)      = F_if(Layer_End(k)+1);

          if FD == 1
             f           = ELECVOLT*Fif(k)*STEPSIZE/Temp/KB;
          else
             f          = 0;
          end

          EA_BarF(k) = abs(EA_Barrier(k)) ;
          IP_BarF(k) = abs(IP_Barrier(k)) ;

% electron
  if EA_Barrier > 0
      n_reverse(Index_Interface(k)+1) = ...
n_reverse(Index_Interface(k)+1)   * ...
exp(-EA_BarF(k)*ELECVOLT/KB/Temp)*exp(sqrt(f)) ;
  else
      n_forward(Index_Interface(k))   = ...
n_forward(Index_Interface(k))    * ...
exp(-EA_BarF(k)*ELECVOLT/KB/Temp)*exp(sqrt(f));
  end

  % hole
  if IP_Barrier > 0
      p_forward(Index_Interface(k))   = ...
p_forward(Index_Interface(k))    * ...
exp(-IP_BarF(k)*ELECVOLT/KB/Temp)*exp(sqrt(f));
```

```
   else
        p_reverse(Index_Interface(k)+1) = ...
p_reverse(Index_Interface(k)+1)   * ...
exp(-IP_BarF(k)*ELECVOLT/KB/Temp)*exp(sqrt(f));
   end

end

       Jp(StepsC)     =  ELECVOLT * ...
(p_forward(StepsC)-p_reverse(StepsC+1))*STEPSIZE;
       Jn(StepsC)     = -ELECVOLT * ...
(n_forward(StepsC)-n_reverse(StepsC+1))*STEPSIZE;

end
```

Bibliography

1 S.-Y. Kim, W.-I. Jeong, C. Mayr, Y.-S. Park, K.-H. Kim, J.-H. Lee, C.-K. Moon, W. Brütting, and J.-J. Kim, Advanced Functional Materials **23,** 3896 (2013).

2 M. A. Baldo, D. F. O'Brien, Y. You, A. Shoustikov, S. Sibley, M. E. Thompson, and S. R. Forrest, Nature **395,** 151 (1998).

3 H. Uoyama, K. Goushi, K. Shizu, H. Nomura, and C. Adachi, Nature **492,** 234 (2012).

4 P. Langevin, Ann. Chim. Phys. **28,** 433 (1903).

5 W. Shockley and W. T. Read, Physical Review **87,** 835 (1952).

6 H. T. Nicolai, M. Kuik, G. A. Wetzelaer, B. de Boer, C. Campbell, C. Risko, J. L. Bredas, and P. W. Blom, Nat Mater **11,** 882 (2012).

7 M. M. Mandoc, B. de Boer, G. Paasch, and P. W. M. Blom, Physical Review B **75,** 193202 (2007).

8 L. J. A. Koster, V. D. Mihailetchi, and P. W. M. Blom, Applied Physics Letters **88,** 052104 (2006).

9 M. Kuik, H. T. Nicolai, M. Lenes, G.-J. A. H. Wetzelaer, M. Lu, and P. W. M. Blom, Applied Physics Letters **98,** 093301 (2011).

10 M. Uchida, C. Adachi, T. Koyama, and Y. Taniguchi, Journal of

Applied Physics **86,** 1680 (1999).

11 W. Shockley, Bell System Technical Journal **28,** 435 (1949).

12 G. Wetzelaer, M. Kuik, H. Nicolai, and P. Blom, Physical Review B **83** (2011).

13 D. Song, S. Zhao, Y. Luo, and H. Aziz, Applied Physics Letters **97,** 243304 (2010).

14 S. Reineke, F. Lindner, Q. Huang, G. Schwartz, K. Walzer, and K. Leo, physica status solidi (b) **245,** 804 (2008).

15 R. Liu, Z. Gan, R. Shinar, and J. Shinar, Physical Review B **83,** 245302 (2011).

16 M. A. Baldo, C. Adachi, and S. R. Forrest, Physical Review B **62,** 10967 (2000).

17 Y. Luo and H. Aziz, Advanced Functional Materials **20,** 1285 (2010).

18 C. Weichsel, L. Burtone, S. Reineke, S. I. Hintschich, M. C. Gather, K. Leo, and B. Lüssem, Physical Review B **86** (2012).

19 J.-H. Lee, S. Lee, S.-J. Yoo, K.-H. Kim, and J.-J. Kim, Advanced Functional Materials **24,** 4681 (2014).

20 M. Kuik, L. J. A. Koster, A. G. Dijkstra, G. A. H. Wetzelaer, and P. W. M. Blom, Organic Electronics **13,** 969 (2012).

21 N. J. Turro, *Modern Molecular Photochemistry* (University Science

Books, 1978).

22 Y.-S. Park, S. Lee, K.-H. Kim, S.-Y. Kim, J.-H. Lee, and J.-J. Kim, Advanced Functional Materials **23,** 4914 (2013).

23 A. Endo, M. Ogasawara, A. Takahashi, D. Yokoyama, Y. Kato, and C. Adachi, Adv Mater **21,** 4802 (2009).

24 K.-H. Kim, C.-K. Moon, J.-H. Lee, S.-Y. Kim, and J.-J. Kim, Adv Mater **26,** 3844 (2014).

25 H. Shin, J. H. Lee, C. K. Moon, J. S. Huh, B. Sim, and J. J. Kim, Adv Mater **28,** 4920 (2016).

26 J.-H. Lee, S.-H. Cheng, S.-J. Yoo, H. Shin, J.-H. Chang, C.-I. Wu, K.-T. Wong, and J.-J. Kim, Advanced Functional Materials **25,** 361 (2015).

27 J.-H. Lee, G. Sarada, C.-K. Moon, W. Cho, K.-H. Kim, Y. G. Park, J. Y. Lee, S.-H. Jin, and J.-J. Kim, Advanced Optical Materials **3,** 211 (2015).

28 K.-H. Kim, S. Lee, C.-K. Moon, S.-Y. Kim, Y.-S. Park, J.-H. Lee, J. Woo Lee, J. Huh, Y. You, and J.-J. Kim, Nat Commun **5,** 4769 (2014).

29 J.-M. Kim, C.-H. Lee, and J.-J. Kim, Applied Physics Letters **111,** 203301 (2017).

30 A. Moliton and J.-M. Nunzi, Polymer International **55,** 583 (2006).

31 N. F. Mott and R. W. Gurney, *Electronic processes in ionic crystals*

(Oxford University Express, 1940).

32 M. A. Lampert and P. Mark, *Current injection in solids* (Academic Press, 1970).

33 G.-J. A. H. Wetzelaer and P. W. M. Blom, NPG Asia Materials **6,** e110 (2014).

34 P. de Bruyn, A. H. P. van Rest, G. A. H. Wetzelaer, D. M. de Leeuw, and P. W. M. Blom, Physical Review Letters **111** (2013).

35 P. Kordt, J. J. M. van der Holst, M. Al Helwi, W. Kowalsky, F. May, A. Badinski, C. Lennartz, and D. Andrienko, Advanced Functional Materials **25,** 1955 (2015).

36 A. Miller and E. Abrahams, Physical Review **120,** 745 (1960).

37 H. Bässler, physica status solidi (b) **175,** 15 (1993).

38 M. Casalegno, C. Carbonera, S. Luzzati, and G. Raos, Organic Electronics (2012).

39 P. Kordt and D. Andrienko, J Chem Theory Comput **12,** 36 (2016).

40 F. Symalla, P. Friederich, A. Masse, V. Meded, R. Coehoorn, P. Bobbert, and W. Wenzel, Phys Rev Lett **117,** 276803 (2016).

41 S. Altazin, S. Züfle, E. Knapp, C. Kirsch, T. D. Schmidt, L. Jäger, Y. Noguchi, W. Brütting, and B. Ruhstaller, Organic Electronics **39,** 244 (2016).

42 S. Züfle, S. Altazin, A. Hofmann, L. Jäger, M. T. Neukom, W. Brütting, and B. Ruhstaller, Journal of Applied Physics **122,** 115502 (2017).

43 J. Staudigel, M. Stossel, F. Steuber, and J. Simmerer, Journal of Applied Physics **86,** 3895 (1999).

44 M. R. Belmont, Thin Solid Films **28,** 149 (1975).

45 H. A. Bethe, in *Semiconductor Devices: Pioneering Papers* (WORLD SCIENTIFIC, 2017), p. 387.

46 J. C. Scott and G. G. Malliaras, Chemical Physics Letters **299,** 115 (1999).

47 J. C. Scott, Journal of Vacuum Science & Technology A: Vacuum, Surfaces, and Films **21,** 521 (2003).

48 C.-C. Lee, M.-Y. Chang, P.-T. Huang, Y. C. Chen, Y. Chang, and S.-W. Liu, Journal of Applied Physics **101,** 114501 (2007).

49 V. Cleave, G. Yahioglu, P. L. Barny, R. H. Friend, and N. Tessler, Advanced Materials **11,** 285 (1999).

50 V. Cleave, G. Yahioglu, P. L. Barny, D.-H. Hwang, A. B. Holmes, R. H. Friend, and N. Tessler, Advanced Materials **13,** 44 (2001).

51 P. A. Lane, L. C. Palilis, D. F. O’Brien, C. Giebeler, A. J. Cadby, D. G. Lidzey, A. J. Campbell, W. Blau, and D. D. C. Bradley, Physical Review B **63** (2001).

52 A. J. Mäkinen, I. G. Hill, and Z. H. Kafafi, Journal of Applied Physics **92,** 1598 (2002).

53 X. Gong, J. C. Ostrowski, D. Moses, G. C. Bazan, and A. J. Heeger, Advanced Functional Materials **13,** 439 (2003).

54 R. J. Holmes, B. W. D'Andrade, S. R. Forrest, X. Ren, J. Li, and M. E. Thompson, Applied Physics Letters **83,** 3818 (2003).

55 A. Kadashchuk, S. Schols, A. Vakhnin, J. Genoe, and P. Heremans, Chemical Physics **358,** 147 (2009).

56 M. Kuik, L. J. A. Koster, G. A. H. Wetzelaer, and P. W. M. Blom, Physical Review Letters **107** (2011).

57 D. C. Hoesterey and G. M. Letson, Jornal of Physics and Chemistry of Solids **24,** 1609 (1963).

58 U. Wolf, H. Bassler, P. M. Borsenberger, and W. T. Gruenbaum, Chemical Physics **222,** 259 (1997).

59 H. Yersin, Top Curr Chem **241,** 1 (2004).

60 M. A. Baldo, S. Lamansky, P. E. Burrows, M. E. Thompson, and S. R. Forrest, Applied Physics Letters **75,** 4 (1999).

61 Z. Q. Gao, B. X. Mi, H. L. Tam, K. W. Cheah, C. H. Chen, M. S. Wong, S. T. Lee, and C. S. Lee, Advanced Materials **20,** 774 (2008).

62 W. S. Jeon, T. J. Park, S. Y. Kim, R. Pode, J. Jang, and J. H. Kwon,

Organic Electronics **10,** 240 (2009).

63 S. Shi, F. Gao, Z. Sun, Y. Zhan, M. Fahlman, and D. Ma, J. Mater. Chem. C **3,** 46 (2015).

64 M. J. Frisch, G. W. Trucks, H. B. Schlegel, G. E. Scuseria, M. A. Robb, J. R. Cheeseman, G. Scalmani, V. Barone, B. Mennucci, G. A. Petersson, H. Nakatsuji, M. Caricato, X. Li, H. P. Hratchian, A. F. Izmaylov, J. Bloino, G. Zheng, J. L. Sonnenberg, M. Hada, M. Ehara, K. Toyota, R. Fukuda, J. Hasegawa, M. Ishida, T. Nakajima, Y. Honda, O. Kitao, H. Nakai, T. Vreven, J. A. Montgomery Jr., J. E. Peralta, F. Ogliaro, M. J. Bearpark, J. Heyd, E. N. Brothers, K. N. Kudin, V. N. Staroverov, R. Kobayashi, J. Normand, K. Raghavachari, A. P. Rendell, J. C. Burant, S. S. Iyengar, J. Tomasi, M. Cossi, N. Rega, N. J. Millam, M. Klene, J. E. Knox, J. B. Cross, V. Bakken, C. Adamo, J. Jaramillo, R. Gomperts, R. E. Stratmann, O. Yazyev, A. J. Austin, R. Cammi, C. Pomelli, J. W. Ochterski, R. L. Martin, K. Morokuma, V. G. Zakrzewski, G. A. Voth, P. Salvador, J. J. Dannenberg, S. Dapprich, A. D. Daniels, Ö. Farkas, J. B. Foresman, J. V. Ortiz, J. Cioslowski, and D. J. Fox, (Gaussian, Inc., Wallingford, CT, USA, 2009).

65 R. R. Chance, A. Prock, and R. Silbey, in *Advances in Chemical Physics* (John Wiley & Sons, Inc., 2007), p. 1.

66 J. A. E. Wasey and W. L. Barnes, Journal of Modern Optics **47,** 725 (2000).

67 J. Chen and D. Ma, Journal of Applied Physics **95,** 5778 (2004).

68 L. Zhang, B. Li, L. Zhang, S. Yue, Q. Xue, and S. Liu, Journal of The Electrochemical Society **158,** J243 (2011).

69 V. Savvateev, A. Yakimov, and D. Davidov, Advanced Materials **11,** 519 (1999).

70 C. W. Ma, O. Lengyel, J. Kovac, I. Bello, C. S. Lee, and S. T. Lee, Chemical Physics Letters **397,** 87 (2004).

71 S. V. Novikov and A. V. Vannikov, Chemical Physics Letters **182,** 598 (1991).

72 D. H. Dunlap, P. E. Parris, and V. M. Kenkre, Physical Review Letters **77,** 542 (1996).

73 C. Lee, S.-K. Park, M. Yang, N.-S. Lee, and N. Kim, Chemical Physics Letters **422,** 106 (2006).

74 C. Groves, L. J. A. Koster, and N. C. Greenham, Journal of Applied Physics **105,** 094510 (2009).

75 L. J. A. Koster, Physical Review B **81** (2010).

76 R. H. Young, Philosophical Magazine B **72,** 435 (1995).

77 L. B. Schein and A. Tyutnev, The Journal of Physical Chemistry C **115,**

6939 (2011).

78 M. Bouhassoune, S. L. M. v. Mensfoort, P. A. Bobbert, and R. Coehoorn, Organic Electronics **10,** 437 (2009).

79 W. F. Pasveer, J. Cottaar, C. Tanase, R. Coehoorn, P. A. Bobbert, P. W. M. Blom, D. M. de Leeuw, and M. A. J. Michels, Physical Review Letters **94,** 206601 (2005).

80 S. V. Novikov and A. V. Vannikov, The Journal of Physical Chemistry C **113,** 2532 (2009).

81 S. V. Novikov, D. H. Dunlap, V. M. Kenkre, P. E. Parris, and A. V. Vannikov, Physical Review Letters **81,** 4472 (1998).

82 C. Li, L. Duan, H. Li, and Y. Qiu, The Journal of Physical Chemistry C **118,** 10651 (2014).

83 C. Li, L. Duan, Y. Sun, H. Li, and Y. Qiu, The Journal of Physical Chemistry C **116,** 19748 (2012).

84 M. Mesta, M. Carvelli, R. J. de Vries, H. van Eersel, J. J. van der Holst, M. Schober, M. Furno, B. Lussem, K. Leo, P. Loebl, R. Coehoorn, and P. A. Bobbert, Nat Mater **12,** 652 (2013).

85 C. Tonnele, M. Stroet, B. Caron, A. J. Clulow, R. C. R. Nagiri, A. K. Malde, P. L. Burn, I. R. Gentle, A. E. Mark, and B. J. Powell, Angew Chem Int Ed Engl **56,** 8402 (2017).

86 R. Coehoorn and P. A. Bobbert, in *Physics of Organic Semiconductors* (Wiley-VCH Verlag GmbH & Co. KGaA, 2012), p. 155.

87 H. Nakanotani, T. Higuchi, T. Furukawa, K. Masui, K. Morimoto, M. Numata, H. Tanaka, Y. Sagara, T. Yasuda, and C. Adachi, Nat Commun **5,** 4016 (2014).

초 록

재결합 현상은 유기 광전자 소자의 구동에 직접적으로 연관된 핵심적인 현상이다. 유기발광다이오드 (OLED)의 경우, 재결합은 광자를 생성하는 엑시톤을 형성하여 발광에 기여하며, 유기 광전지 (OPV)의 경우 재결합은 광자에 의해 생성된 에너지가 손실되기 때문에 최소화 해야할 현상이다. 유기 반도체에서 고려되는 두 가지의 주요한 재결합 메커니즘이 있다. 하나는 정공과 전자 사이에서 발생하는 랑제빈 재결합 현상이며, 다른 하나는 트래핑 된 전하와 반대 부호의 전하 사이에 발생하는 트랩 보조 재결합 현상이다. 각 메커니즘이 미치는 영향은 소자 종류에 따라 다르지만, 이러한 현상을 원인을 파악하고 이해하는 것은 소자의 성능을 향상시키는데 공통적으로 중요하다. 이 논문에서 연구한 염료 도핑된 OLED 시스템에서는, 재결합 메커니즘은 구동 전압 및 효율을 결정짓는 중요한 요소이다. 이러한 중요성에도 불구하고 재결합 메커니즘을 결정하는 요인에 대한 연구는 많이 이루어지지 않았다. 트랩 심도의 효과가 그 중 하나 이지만, 깊은 트랩 준위를 가지는 시스템에서도 랑제빈 재결합 현상이 지배적인 시스템을 구축하는 것이 가능하다고 보고되었으며, 이러한 현상을 설명할 수 있는 이론에 대한 연구가 필요

하다.

이 논문에서는 첫번째로, 엑시플렉스 형성 공동 호스트 시스템 구조의 가상 소자를 연구 하였다. 층간 장벽 효과, 발광층의 전하 이동도 및 트랩 심도에 따라 표동−확산 모델링을 이용하여 소자에서의 전하 밀도, 재결합 속도 및 랑제빈 재결합 비율을 계산하였다. 그 결과 발광층의 전하이동도가 낮아질수록, 층간 에너지 장벽의 크기가 커질수록 발광층에서 정공 또는 전자 더 축적된다는 결과를 얻었으며, 이로 인해 소자에서의 랑제빈 재결합의 비율이 증가된다는 사실을 밝혔다. 또한 트랩 심도의 경우, 트랩을 빠져나가는 현상에 영향을 주어 트랩된 정공의 밀도와 관련이 있으며, 트랩 심도가 0.3 eV 이상으로 커질 경우, 이 파라미터의 크기에 상관없이 일정해 진다는 사실을 알았다. 이 결과를 엑시플렉스 공동 호스트에 대응시켜 볼 때, 이러한 구조가 랑제빈 재결합이 우세한 시스템을 만들기에 적합한 호스트 라는 사실을 알 수 있었다.

두 번째로, 도펀트의 쌍극자 모멘트가 염료로 도핑된 OLED의 재결합 메커니즘에 영향을 미치는 가장 중요한 요인 중 하나임을 밝혔다. 우선, 전류−전압 및 시간 전계 발광 특성을 통하여, 5 Debye 이상의 큰 쌍극자 모멘트를 가진 동종 리간드 구조의 이리듐 발광체는 트랩 보조 재결합에 의한 발광 현상을 가진다는 것을, 그러나 2 Debye 미만의 작은 쌍극자 모멘트를 갖는 이종 리간드의 이리듐

발광체는 랑제빈 재결합에 의한 발광 특성을 가진다는 것을 밝혔다. 또한 우리는 표동–확산 모델에서 쌍극자 모멘트의 트랩 효과를 추가적으로 고려하여, 트랩 깊이가 0.25 eV 보다 큰 경우 트랩 깊이에 의한 효과는 무시 가능하며, 쌍극자 모멘트가 소자의 재결합 메커니즘을 결정짓는 중요한 요인이 된다는 것을 밝혀냈다. 이 발견은 형광 또는 열활성 지연 형광 OLED를 포함하여 다양한 종류의 OLED 연구에 유용할 것으로 예측된다.

주요어: 재결합, 표동-확산 모델, 랑제빈 재결합, 트랩 보조 재결합, 발광체의 쌍극자 모멘트
학 번: 2013-30185

CURRICULUM VITAE

Lee, Chang-Heon
Department of Materials Science and Engineering
Seoul National University, Seoul, 151-744, Korea
+82-2-875-2412 (Office)
E-mail: ilios8818@snu.ac.kr

Education

2013.03 ~ 2018.02	**Ph.D** in Materials Science and Engineering Supervisor: Professor Jang-Joo Kim Seoul National University, Seoul, Korea
2011.03 ~ 2013.02	**M.S** in Materials Science and Engineering Supervisor: Professor Jang-Joo Kim Seoul National University, Seoul, Korea
2007.03 ~ 2011.02	**B.S.** in Materials Science and Engineering Seoul National University, Seoul, Korea

Research Interests

- Electrical modeling of organic light emitting diodes
- Electrical transport characteristics in organic semiconductors
- Organic electronic devices (OLEDs, OPVs)
- Recombination mechanism in OLEDs

Professional Skills

- Electrical modeling of organic devices (OLED, OPV) with drift-diffusion modeling

- Optical modeling of organic devices (OLED, OPV) with transfer-matrix method
- Design and fabrication of organic electronic devices (OLED, OPV) with vacuum thermal evaporator
- Mobility measurement with time-of-flight (TOF) equipment
- Impedance spectroscopy, UV-vis-NIR absorption spectroscopy, OLEDs characteristic measurements (J-V, Transient photoluminescence (PL) & electroluminescence (EL), PL efficiency measurement

List of publication

1. **Chang-Heon Lee**, Jeong-Hwan Lee, Kwon-Hyeon Kim and Jang-Joo Kim*, “Unveiling the Role of Dopant Polarity on the Recombination and Performance of Organic Light-Emitting Diodes”, Advanced Functional Materials (2018, accepted)
2. Jae-Min Kim, **Chang-Heon Lee**, Jang-Joo Kim*, "Mobility balance in the light-emitting layer governs the polaron accumulation and operational stability of organic light-emitting diodes", Applied Physics Letters **111**, 203301 (2017)
3. Hyun-Sub Shim, Sei-Yong Kim, Ji Whan Kim, Tae-Min Kim, **Chang-Heon Lee**, Jang-Joo Kim*, "An efficient interconnection unit composed of electron-transporting layer/metal/p-doped hole-transporting layer for tandem organic photovoltaics", Applied Physics Letter **102**, 203903 (2013)